Astral microtubule dynamics regulate anaphase oscillation onset and set a robust final position of the *C. elegans* zygote spindle.

H. Bouvrais[1,2,*], L. Chesneau[1,2], S. Pastezeur[1,2], M. Delattre[3], J. Pécréaux[1,2,*]

Affiliations

1) CNRS UMR 6290, 2 avenue du Professeur Léon Bernard, CS 34317, F35043 Rennes cedex, France.
2) University Rennes 1, UEB, SFR Biosit, School of medicine, F-35043 Rennes, France
3) Laboratory of Molecular Biology of the Cell, Ecole Normale Supérieure de Lyon, CNRS, Lyon, France

Contact info

* = helene.bouvrais@univ-rennes1.fr, jacques.pecreaux@univ-rennes1.fr

Graphical Abstract

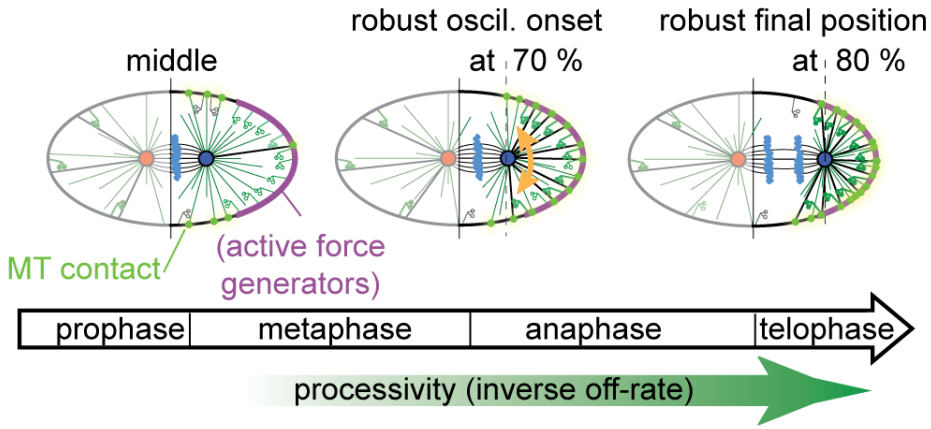

Abstract

Background: The correct positioning of the mitotic spindle during the asymmetric division of the nematode *C. elegans* zygote relies on the combination of centering and cortical–pulling forces. These forces, revealed by centrosome anaphase oscillations, are regulated through the dynamics of force generators, related to mitosis progression. Recently, we reported the control of oscillation onset by the posterior spindle pole position in related species *C. briggsae*, necessitating a re-evaluation of the role of astral microtubules dynamics. **Results:** After exhibiting such a positional switch in *C. elegans*, we mapped the microtubule ends at the cortex and observed a correlation between the proximity of the centrosomes and the density of microtubule contacts. To explore the functional consequences, we extended the "tug–of–war" model and successfully accounted for the positional switch. We predicted and experimentally validated that the control of oscillation onset was robust to changes in cell geometry or maximum number of attached force generators. We also predicted that the final position of the posterior centrosome and thus the spindle has a reduced dependence upon the force generator dynamics or number. **Conclusion:** The outburst of forces responsible of spindle anaphase oscillations and positioning is regulated by the spindle position through the spatial modulation of microtubule contacts at the cortex. This regulation superimposes that of force generator processivity putatively linked to the cell cycle. This novel control provides robustness to variations in zygote geometry or detailed properties of cortical force generators.

Highlights

- Microtubule contacts at the cortex concentrate at regions close to the centrosomes.
- This regulates pulling forces and creates a positional switch on oscillation onset.
- The onset position is robust to changes in embryo length or force generator dynamics.
- The final centrosome position is robust to changes in generator number or dynamics.

eTOC Blurb

Observing inhomogeneous MT contact density at cortex, Bouvrais et al. propose that the posterior centrosome position regulates engagement of pulling force generators, creating a positional switch on oscillation onset. This, and thus final centrosome position, is robust to variation in number or dynamics of force generators.

Running title:

Space and time regulation of the spindle positioning

Keywords:

Microtubule dynamics, sub cellular force regulation, positional regulation, robust positioning. Cell division, cell mechanics, robustness, optical microscopy and image processing.

Introduction

Asymmetric cell divisions, in which daughter cell sizes, content and fates differ, are essential to the development of multicellular organisms [1, 2]. In the nematode *Caenorhabditis elegans* [3] as in many other species [4, 5], the mitotic spindle contributes to positioning the cytokinesis furrow. It needs to be oriented along the polarity axis [6] and in some cases displaced out of cell center prior to cytokinesis to correspond to cortical polarity cues [6, 7]. Pulling forces, exerted on the plus-end of astral microtubules from the cell cortex, are common to most asymmetric divisions and play a key role in positioning and orienting the spindle [6-8].

In the nematode one-cell embryo, cortical forces are generated by a well–conserved trimeric complex, which pulls on astral microtubules, and which comprises a dynein/dynactin complex, a NuMA homolog LIN-5 and a G-protein regulators GPR-1/2, homolog of mammalian LGN [9]. In such an asymmetric division, GPR-1/2 translate polarity cues [10] through their asymmetric localization [11, 12], increasing the number of active force generators locally. Prior to the cell division, during the centering phase [13], GPR-1/2 contribute to orienting the spindle along the anteroposterior axis (AP-axis) and displace the pronuclei centrosomes complex (PCC) from the posterior side of the embryo, where pronuclei have met, to a slightly anterior position (overcentration) [12, 14]. During prometaphase and metaphase, centering forces independent of GPR-1/2 and putatively due to microtubules pushing against the cell cortex, maintain the spindle in the center [15]. GPR-1/2–dependent cortical pulling forces become dominant in late metaphase and anaphase displacing the spindle posteriorly, making it rock and contributing to its elongation [16-18].

The activity of the cortical force generators is regulated in three different ways: firstly, in space through modulation across the various cortical regions in response to polarity cues: the rate of force generators binding to astral microtubules [19] is increased in the posterior half during metaphase and anaphase, leading to twice more *active* force generators in the posterior cortex compared to the anterior one, in the region marked by the PAR-2 polarity protein [10, 16, 20]. However, such an active region spans only from 70 % of the anteroposterior axis (AP axis) to the posterior tip of the embryo because the force generator activity is diminished in the middle region (from 40 % to 70 % of the AP-axis) by the LET-99 protein [21, 22]. Secondly, the number of active force generators is regulated in time and increases during cell division [17], possibly depending on the cell cycle [23]. We found that the spindle anaphase rocking and posterior displacement were accounted for by a decrease of force generator off-rate from microtubules throughout the anaphase, resulting in a global increase of pulling forces [18] (SI text § 2.2.1). Our original "tug-of-war" physical model assumed however that astral microtubules were abundant at the cortex during anaphase and that the sole limiting factor was the force generators binding/unbinding dynamics. Such a microtubule abundance, likely true during anaphase, is questionable in earlier phases. Thirdly, microtubule dynamics can play a role in regulating the cortical pulling forces [24]. Kozlowski and co-authors proposed an alternative model in which the limited access of microtubules to the cortex could account for spindle oscillations [25]. Microtubule contact durations at the cell cortex appeared modulated between anterior and posterior sides [24]. Microtubule dynamics could also be a mean of time regulation through its increase along the course of the cell division [26].

Previous studies have underlined the key role of microtubules in microtubule organizing center (MTOC) positioning. Indeed, they are able to "sense" the cell geometry, for example to bring MTOC at the cell center [27, 28], or to orient the nucleus by exerting pulling forces that scale with microtubule length [29]. Similarly, in HeLa cells, microtubules "integrate" the adhesive pattern, whose cues are cortical, to orient the spindle accordingly [30]. In the *C. elegans* embryo, microtubules may contribute to orient the spindle together with polarity cues reading its oblong shape [31]. We therefore asked whether the modulation of the microtubule contacts in various regions of the cortex could modulate the cortical force generation.

We recently observed that anaphase spindle oscillation onset, and thus pulling forces, was controlled by the position of the posterior spindle pole rather than by mitosis progression in *C. briggsae*. Indeed, oscillations start when the posterior pole reaches 70 % of the AP-axis in two nematode species (*C. elegans* and *C. briggsae*), which have diverged 100 million years ago. Interestingly, this position was reached 30 s after anaphase onset in *C. briggsae* and simultaneously to it in *C. elegans*. Knowing that the amount of GPR-1/2 is key to regulate cortical pulling forces [10, 16], this robust onset of oscillations was even more striking considering that GPR was duplicated only in *C. elegans* and that GPR sequences have diverged

between the two species [12]. These observations suggested that a positional switch controls pulling forces. We propose here that such a switch relates to microtubule dynamics.

Measuring the residency time of microtubules at the cell cortex along the course of the mitosis was key to exploring such a hypothesis. Indeed, while the dynamics of the microtubules in the cytoplasm, and its time-evolution, are quite clear in the nematode embryo [26], the time they spend at the cortex is more elusive with published values ranging from second [25] to more than ten seconds [24]. Such a discrepancy can be explained by the very fast dynamics of microtubules calling for imaging at high frame rates. In this paper, we carefully measured the space modulation of such dynamics. We used these measurements to decipher the regulatory role of microtubule dynamics on cortical pulling forces, accounting for the decoupling between oscillation and anaphase onsets observed in *C. briggsae* [12], and here in *C. elegans*. We extended our original "tug–of–war" model, focused on force generator dynamics, to account for this microtubule–dynamics–related positional switch of cortical pulling forces. We challenged this model with experiments comparing both predicted and experimental robustness of the switch to embryo shape perturbations or to the force generator active region boundary. Reasoning on posterior displacement and using an *in silico* approach, we explored the consequences on the spindle positioning regulation and especially on the spindle final position, which contributes to setting the cytokinesis furrow position.

Results

Spindle oscillations can start before anaphase onset in *C. elegans*.

We previously reported that the position of the posterior pole of the spindle controls the onset of the spindle oscillations in *C. briggsae* [12]. We asked whether the simultaneous anaphase and oscillation onsets observed in *C. elegans* were coincidental. We delayed the anaphase using a *such-1*^{ANAPC5}*(h1960)* mutant of anaphase promoting complex/cyclosome (APC/C) [32], labelling centrosomes and chromosomes through SPD-2^{CEP192}::GFP;HIS-58^{H2B}::mcherry. We tracked the centrosomes [15, 18] and observed precocious oscillations with respect to anaphase onset (Table 1). The oscillations started when the posterior centrosome was at 70 % of embryo length, both in control and mutant, as in *C. briggsae* [12]. In contrast, for both mutant and control, the oscillation die–down happened about 2 minutes after anaphase onset, disregarding the timing of their onset leading to variations in their duration (Table 1). We concluded that a positional switch controls anaphase oscillation onset in *C. elegans* embryos while their end depends on the cell cycle. In the following, this assay based on centrosome tracking has been instrumental to functionally test the positional switch.

Characteristic measured (mean ± s.e.m.)	control (N=17)	such-1(h1960) (N=15)
Oscillation onset T1 (s)	-11.03 ± 5.50	-39.83 ± 5.93 p=9 x 10-4
Posterior centrosome reached 70% AP-axis T2 (s)	-11.76 ± 5.68	-85.50 ± 17.15 p=6 x 10-4
Oscillations onset to reaching of 70% delay T1-T2 (s)	0.74 ± 4.96	45.67 ± 15.82 p=0.015
Maximum oscillation amplitude (posterior) (%)	20.78 ± 0.65	22.71 ± 0.61 p=0.035
Nuclear Envelope Breakdown (s)	- 164.84 ± 3.48	- 291.04 ± 5.40 p=1 x 10-17
Oscillation die-down T3 (s)	124.4 ± 7.0	117.5 ± 7.63 p=0.507
Oscillation duration T3-T1 (s)	135.4 ± 8.9	157.3 ± 9.7 p=0.11
Posterior centrosome position at oscillation onset (%)	70.68 ± 0.89	70.76 ± 0.49 p=0.936
Posterior centrosome position when oscillation died down (%)	79.51 ± 0.40	79.01 ± 0.69 p=0.515
Embryo length (µm)	52.60 ± 0.86	53.98 ± 0.80 p=0.237
Embryo width (µm)	35.21 ± 0.61	33.25 ± 0.53 p=0.019

Table 1: Timing and position of metaphase and anaphase events, in untreated embryos and delayed anaphase mutants. SPD-2^{CEP192}::GFP;HIS-58^{H2B}::mcherry labelled embryos were imaged at 18°C and spindle poles tracked. We compared untreated embryos with *such-1(h1960)* mutants, a gene coding for APC/C, homolog of ANAPC5 [32]. Times were measured with respect to the anaphase onset and amplitude of oscillations peak to peak in % of embryo width. Positions along the AP-axis are in % of embryo length. Error bars are s.e.m. p values are reported for Student's t-test.

Microtubule contacts at the cortex depend upon centrosome position.

To account for this positional switch, we hypothesized that the network of astral microtubules emanating from the posterior centrosome could have reduced accessibility to the posterior crescent of the cortex, where are located the active force generators [22], and further termed the active region. When the spindle is close to the cell center, the density of microtubule contacts in the active region would be very low (graph. abstract, *left*); this density would increase as the posterior centrosome is displaced toward the posterior (graph. abstract, *middle* and *right*). The oscillations, which build up above a threshold number of active force generators, would depend on the position of the centrosome. We challenged our hypothesis by measuring directly the spatial distribution of the microtubule contacts at the cortex. We preserved the embryo shape by using spinning disk microscopy and measuring microtubule dynamics through α-tubulin rather than EB labelling (see Suppl. Exp. Proc., S1A). Because microtubule dynamics are fast, we imaged microtubule contacts at the cortex at 10 frames per second. Our method correctly recovered an exponential distribution of the residency times (Fig. S1B) consistent with previously published values [25]. We computed the distribution of the microtubule contacts along the anteroposterior axis. To gain certainty, we block–averaged the distribution in 10 regions distributed along the AP-axis and performed a running time–average with a 10 s window. We observed spatial heterogeneity, in particular ridge lines, and an overall increase of the number of contacts between metaphase and anaphase consistent with the increasing nucleation rate measured previously [26] (Fig. S1C). To test whether the ridge lines corresponded to the centrosome position, we imaged the spindle plane in the same strain and temperature with a wide–field microscope. We tracked the centrosomes as previously described [18]. We combined the results of both experiments and aligned them with anaphase onset (see Suppl. Exp. Proc.). We found that centrosome positions coincided with the ridge lines delineated by the highest microtubule density regions (Fig. 1). Because we initially observed a positional switch on cortical pulling forces in one-cell *C. briggsae* embryos [12], apparently related to the modulation of microtubules cortical contacts, we performed the same experiments in this species and obtained similar results (Fig. S2). We concluded that the distance of the centrosome to the cortex strongly modulates the number of microtubule end contacts in both species. As a consequence, the number of contacts in the active region increased with the posterior displacement of the spindle.

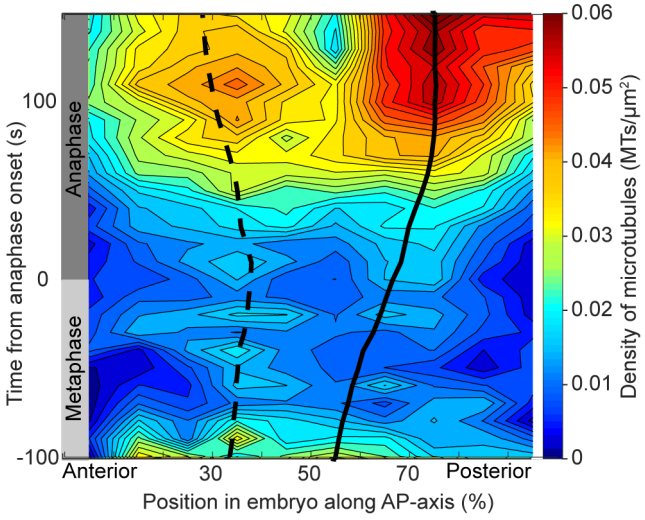

Figure 1: Microtubule contact density at the cell cortex in *C. elegans*.

Microtubule contact density at the cortex obtained by spinning disk microscopy by imaging a YFP::α-tubulin strain (see Methods), averaged along the AP-axis (in 10 regions of equal width) and along time (10 s running window) and represented by a heat map (N=22 *C. elegans* embryos). The centrosome trajectories, obtained by imaging the same strain in the spindle plane, were superimposed (N=8 *C. elegans* embryos). Dashed line represents the anterior centrosome trajectory, solid line the posterior. Time was measured from anaphase onset.

A comprehensive model for pulling force regulation and spindle oscillations

We expected the modulation of microtubule contact density by the centrosome–to–cortex distance to regulate the cortical pulling forces and to create the positional switch that we previously observed. Indeed, we reported on *C. briggsae* at anaphase onset [12] and observed here (Table 1) that when the posterior centrosome was not localised posteriorly enough, it led to a reduced cortical density of microtubules and a number of active force generators below the threshold required for oscillations [18], thus delaying anaphase oscillations. Such a putative positional control of oscillation onset contrasted with the original "tug-of-war" hypothesis, which posits that both the build up and die down timings were regulated by the processivity of force generators [18], possibly related to mitosis progression [23]. To challenge this hypothesis, we extended the original "tug–of–war" model to quantitatively capture how the microtubule network could create a positional switch on cortical pulling forces.

Extending the model to account for microtubule dynamics

We modelled the dynamic instability of microtubules considering that they alternately grow and shrink [33] but neglecting the putative force dependent catastrophe rate [34]. Furthermore, we assumed that catastrophes happen only at the cortex (no free end catastrophe) and that upon shrinking, microtubules fully depolymerize (negligible rescue rate) [25, 26, 35] (SI text §2.1.1). We also set a constant number of microtubule nucleation sites at the centrosomes, which were never empty [34], and from where microtubules emanated with an isotropic angular distribution [26, 36]. We computed the number of microtubules that reached the cortex in the active region (Fig. 2C, *left*, purple color) as a function of the position of the posterior centrosome (Fig. 2A, black curve): we noticed a steeper increase at a position consistent with oscillation onset at 70 % of embryo length. We modelled the embryo as an ellipsoid but our result was independent of that hypothesis: we tested various super-ellipse shapes [37] and found the same switch behavior (SI text § 2.1.3 and Fig. S3). We pursued modelling using an ellipsoid to represent the embryo shape. We concluded that microtubule dynamics, by regulating the number of microtubules available to force generators, can implement the positional switch observed experimentally. Furthermore, the large number of microtubules contacting the active region during mid and late anaphase is consistent with the previous assumption of the original "tug-of-war" model that microtubules saturate a limited number of cortical force generators during this period [18, 38].

Combining with force generator dynamics

To account for the dynamics of force generators, which set oscillation frequency and the timings of their peak amplitude and die down [18], we modelled microtubule binding to the force generators [9], as a first-order chemical reaction using the mass action law (therefore assuming no cooperative binding between force generators when binding) [39], and estimating the association constant from the binding and unbinding rates used in modelling anaphase oscillations [18] (SI text § 2.2.2). For the sake of clarity, we initially assumed a time independent association constant to model the onset of oscillations. This enabled us to compute the number of engaged force generators *versus* the posterior centrosome position (SI text §2.2). We found that when the centrosome was far from the posterior tip, the scarcity of astral microtubule contacts in the active region of the cortex limited the number of engaged force generators below the previously described threshold for oscillations [18] (Fig. 2B, black curve, 2C, *left*). We observed a steep increase in engaged force generators upon posterior displacement of the centrosome above 60% of AP-axis (compare Fig. 2AB, black curves), similar to the number of microtubule contacts, followed by a saturation starting from 70% of AP-axis. This switch–like behavior was consistent with our positional switch hypothesis. The precise position at which oscillations started was dependent on the position of the active region boundary (Fig. 2B). We assumed that this region was set up by LET-99 force generator inhibition [22] and extended from 70 % to 100 % of AP-axis [21] (see experimental validation below). Thus, the positional switch was localized at about 70 % of the AP axis, consistent with our previous experiments. We kept this choice for the positional switch in the further steps. The observed saturation in the number of engaged force generators suggests that their dynamics, rather than number, become the control parameter. This is consistent with the timings of peak and die–down of oscillations being mostly independent of centrosome position but occurring after a delay from anaphase onset (Table 1), as accounted for by the original model. In writing the mass action law in force generator number, we have assumed that the diffusion of the cortical anchor of force generators at the cell membrane is fast enough to not be limiting (SI text § 2.2.4). We checked this assumption by computing the number of engaged force generators *versus* the position of the posterior centrosome, but in this case the microtubule-force generator binding was modelled by the law of mass action in areal concentration, and we found again a positional switch (compare S4AB, black curves). In conclusion, our model suggests that the oscillation onset is specifically regulated by the posterior displacement of the posterior centrosome.

Microtubule and force generator dynamics set two independent switches

We next wondered how processivity (reflecting mitosis progression [18, 23]) and position of the posterior centrosome combined to initiate oscillations. We completed the extended "tug-of-war" model by making the microtubule–force-generator association constant dependent on time through the off-rate (inverse of processivity), as it was the control parameter in the original model; this parameter decreases along the course of mitosis [18] (SI text § 2.2.5). In contrast with the original "tug-of-war" model, the force generator on-rate is not constant and depends here upon the number of microtubules available at the cortex for binding a force generator (SI text § 2.2.2), in addition to its polar regulation [19] (SI text § 3). This suggests that the posterior centrosome needs to be posterior enough to enable oscillations, thus supporting our positional switch experiment (Fig. 2D, blue curve). In addition to this positional control,

the processivity needs to be in a given range (Fig. 2D, blue region), below and above which the oscillations are dampened out (Fig. 2D, white regions), consistent with the control by a steady increase of processivity [18]. This leads to a dual control of pulling forces. Interestingly, the posterior centrosome position more strongly influences oscillation onset (Fig. 2D, blue curve) than oscillation dying down (Fig 2D, green curve with a higher slope than the blue one), as seen experimentally (SI text §2.2.5). In conclusion, we extended the original "tug-of-war" model by adding a positional switch to control oscillation onset and similarly the forces contributing to spindle elongation and posterior displacement.

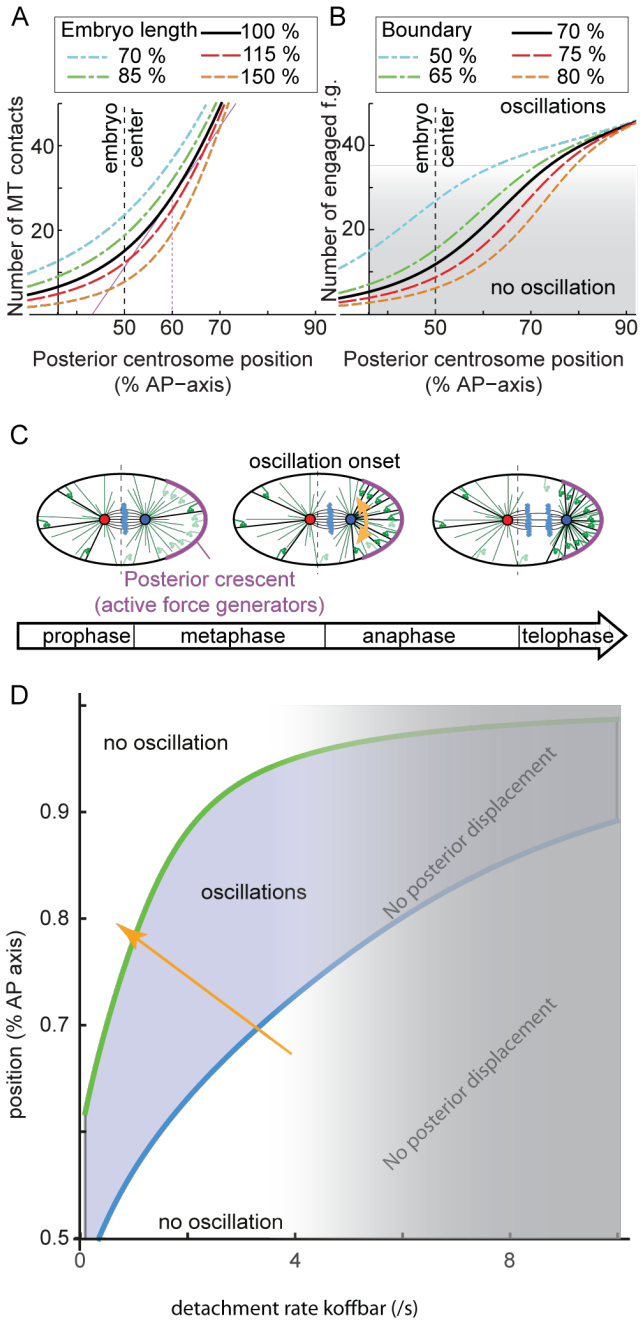

Figure 2: Extended "tug-of-war" model.

(**A**) Modelled number of microtubules (MTs) contacting the cortex in the active region (boundary at 70 % of the current AP-axis) *versus* the posterior displacement of the centrosome along the AP-axis, varying embryo length from 70 to 150 % of untreated one (SI text § 2.1.3). For this latter (thick black line), when the centrosome position was above 60 %, the number of contacts started to increase steeply (purple line). (**B**) Number of engaged force generators (f.g.), i.e. pulling on a microtubule, *versus* the posterior displacement of the centrosome along the AP-axis varying the position of the active region boundary expressed in % of embryo length (SI text § 2.2.2). Thick black line represents a boundary at 70 % mimicking the untreated embryo. In this case, when the centrosome reached 60 % of the AP-axis, the number of engaged force generators increased steeply and saturated above 70 % creating a switch like behavior. Cold–colored curves model *let-99(RNAi)* experiments where the boundary was displaced anteriorly. Hot-colors depict cases of posteriorly displaced boundary. Gray shading depicts conditions where the number of engaged force generators was too low to permit oscillations (below threshold) (**C**) Extended "tug-of-war" schematic representation: at early metaphase, the spindle is roughly centered (*left*), roughly at anaphase onset, it reaches 70 % of AP-axis and starts oscillating (orange arrow, middle panel) and after anaphase, it reaches ~80 % of AP-axis, its final position (*right*). Red and blue disks represent anterior and posterior centrosomes, respectively. Light blue clouds represent the chromosomes. Microtubules that emanate from the centrosomes either: (1) reach the cortex and find an active force generator (thick black lines), (2) reach an inactive region of the cortex or are too short to reach the cortex (thin green lines). Purple cortical region is the posterior crescent where lie the active force generators. Inactive and engaged force generators are represented in light and dark green, respectively. Within the spindle, microtubules are represented by thin black lines. Vertical dashed line marks the middle of the AP-axis. **(D)** Stability diagram of the extended "tug-of-war" model as a function of detachment rate (off-rate $\overline{k_{off}}$, inverse of the processivity, x-axis) and of the position of the centrosome in % of embryo length (y-axis). The unstable region (blue area) corresponds to negative damping Ξ exceeding positive one Γ=140 µN.s/m [40] and oscillations developing (SI text § 2.2.5). The critical values are depicted by the blue and green thick lines. The orange arrow depicts the typical phase–trajectory during a mitosis based on parameters in use in this study. The grayed out area indicates that above a threshold detachment rate, the posterior displacement of the spindle/posterior centrosome no longer happens (Fig. 5). The centrosome needs to reach a posterior enough position to enable oscillations with realistic force generator processivity (measured to 1-2 s^{-1} in metaphase [19]). Furthermore, the inclined entry boundary corresponding to oscillation onset (blue line) suggests that it is under the double control of position and processivity. In contrast, the steep return–to–stability line (green), corresponding to oscillation die down, suggests that die down depends mostly on processivity. For all plots, numerical values of the parameters in use are reproduced in SI text § 4.

We then aimed at validating the model through three experiments: we firstly tested whether the boundary of the active region sets the centrosome position corresponding to oscillation onset; we secondly confirmed that this onset position is not controlled by force generator activity (SI text §2.2.3). Finally, we challenged one prediction of the positional switch stating that the position, in contrast to the timing, of oscillation onset weakly depends on the embryo length.

Position of the active region boundary controls oscillation onset

In building the model, we asserted that the boundary of the active region, in which the active force generators are restricted, controls the position at which oscillation are initiated. Our model predicted that when this region extends more anteriorly, the position at which oscillations start is also displaced anteriorly (Fig. 2B, curve with cold colors). To challenge this prediction, we extended the active region by partially depleting the protein LET-99 by RNAi, which is thought to restrict the force generator regulators GPR-1/2 to the active region [11]. In such a case, the active force generators are thought to extend in the whole posterior half of the embryo [22]. We observed that oscillations started significantly more anteriorly compared to the control (Fig. 3A), in agreement with the model predictions. Interestingly, the oscillations also started earlier with respect to anaphase onset, further supporting that the onset is independent of mitosis progression (Fig. 3B). We concluded that it is likely that the position of the active region boundary controls at which position oscillation onset occurs.

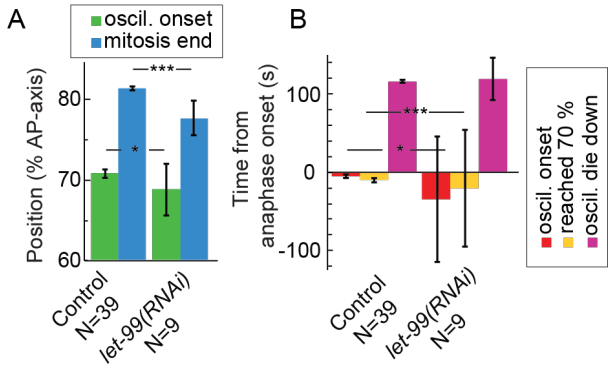

Figure 3: Force generator localization contributes to setting the position switch. (A) Positions of the posterior centrosome at oscillation onset and die down and **(B)** timings of oscillation onset, die down, and reaching 70 % of embryo length upon changing the size of the active region. We measured N=9 *let-99(RNAi)* and N=39 untreated embryos, with centrosomes labelled by GFP::γ-tubulin, at 23°C. Error bars indicate SD and stars indicate significant differences (see methods).

Because the positional switch relies on microtubule dynamics, our extended "tug-of-war" model predicts that the position of oscillation onset is independent of the total number of force generators (Fig. S6A), if this number is above the threshold required for oscillations. We previously suggested experimentally such a result [12] and could successfully repeat it (SI test § 2.2.3).

Reduced sensibility of oscillation onset position with embryo size

Our extended "tug-of-war" model suggested a weak dependence of the position of oscillation onset upon the length of the embryo, particularly to elongation (Fig. 4A). To challenge such an increased robustness with respect to the original model, we depleted C27D9.1 or CID-1 by RNAi to obtain longer or shorter embryos respectively. In both cases, embryos were viable and showed no other visible phenotypes. We measured the variation of the timing and the position of oscillation onset with respect to the variation of the embryo length. We fitted a linear model in both cases and measured the oscillation onset timing slope to be 10 times larger than that of the oscillation onset position (Fig. 4B-C). This further suggests that the position and timing (with respect to anaphase onset) at which the oscillations start are not correlated. This result was also perfectly consistent with the reduced sensitivity of oscillation onset position to the embryo length predicted by the model (Fig. 4A). In contrast, the position at which oscillation die down is impacted by embryo length (Fig. 4D), as expected since it is temporally controlled. We concluded that our extended "tug-of-war" model was supported by these experiments.

Positional oscillation onset sensitivity analysis of the extended model

Using our model, we finally performed a thorough sensitivity analysis (Fig. S5). As expected, the number (Fig. S5F) and dynamics (Fig. S5C) of the microtubules were critical in setting the position of oscillation onset. To a lesser extend, the embryo width (Fig. S5D) and proportional scaling (Fig. S5E) were also influential. Interestingly, as the robustness of the position of oscillation onset *versus* the embryo length suggested (Fig. 4A), the eccentricity, keeping area constant, has a reduced impact (Fig S5B). Similarly, the number (Fig. S6A) or dynamics (Fig. S4A) of the force generators appears to have only a small effect when they reach the threshold to enable oscillations, as previously reported [18]. The cortical distribution of the force generators and their restriction to the active region is also key (Fig. 2B). In conclusion, the positional control of oscillation onset relies on microtubule dynamics, while force generator dynamics are related to polarity translation and likely progression through mitosis by their processivity.

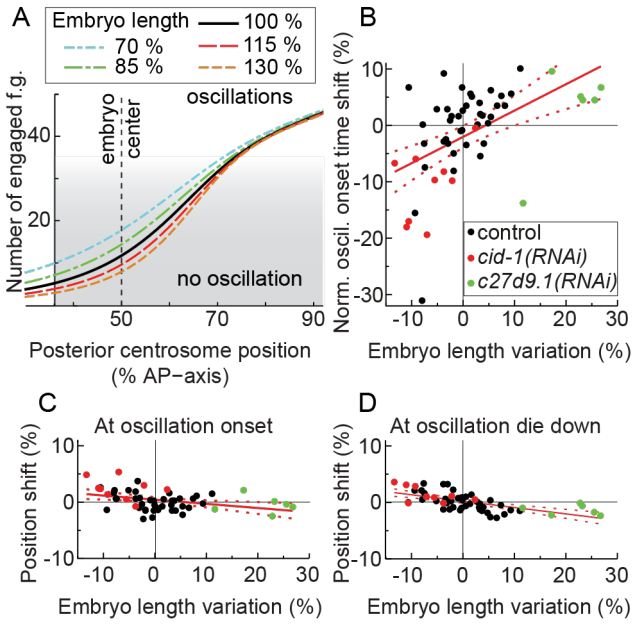

Figure 4: Positions of oscillation onset and die down but not timing have a reduced dependence on the length of the embryos. (A) Modelled number of microtubules (MTs) contacting the active region of the cortex *versus* the posterior displacement of the centrosome along the AP-axis as % of embryo length. The length of the embryo was encoded by the color of the lines, with the black line corresponding to unperturbed embryos and cold colors to shorter ones through *cid-1(RNAi)* and hot colors to longer ones through *c27d9.1(RNAi)*. Numerical parameters in use are reproduced in SI text § 4. Gray shading depicts conditions where the number of engaged force generators was too low to permit oscillations (below threshold). **(B)** Shift of oscillation onset with respect to control normalized by the average duration of pro-metaphase and metaphase in control *versus* the variation of the length of the embryo with respect to control normalized by the average length for control (see Suppl. Exp. Proc.). The red solid line corresponds to least-squares linear fit with slope 0.47±0.11 ($p=5\times10^{-5}$ compared to null slope) and red dashed lines to sem. **(C)** and **(D)** Shifts in position at oscillation onset and die down with respect to control *versus* the normalized shift in embryo length. Linear fit gave slope -0.07±0.02 (p=0.005) and -0.11±0.02 ($p=2.6\times10^{-7}$). We measured N=9 *cid-1(RNAi)*, N=6 *c27d9.1(RNAi)* and N=39 untreated centrosome labelled GFP::γ-tubulin embryos at 23ºC. Dots indicate individual embryos. Thin black lines indicate 0 shift (average values of control).

Astral microtubule dynamics regulate the final position of the spindle

The microtubule dynamics create a feedback on cortical pulling forces, which set the spindle final position.

Cortical pulling forces, which cause the anaphase spindle oscillations, also cause the posterior displacement of the spindle during late metaphase and anaphase [17, 18]. In our original "tug-of-war" model, we suggested that the final posterior centrosome position resulted from the balance between the cortical pulling forces and the centering forces, modelled by a spring [18]. In contrast, in our current model, the averaged number of engaged force generators does not only depend on their dynamics but also on microtubule availability at the cortex, and thus centrosome position. We reasoned that the positional control of the pulling forces generated caused a feedback loop on the final position of the spindle, to which they contributed. To investigate this hypothesis, we simulated the posterior displacement using our extended "tug-of-war" model using the TR-BDF2 algorithm [41] (SI text § 3.1). To have a proper force balance on the spindle, we also included the anterior centrosome using the extended "tug-of-war" model with an active region from 0 to 40 % corresponding to the region devoid of LET-99 [21]. We however kept it to a fixed position. Such a simplification is relevant since the "tug-of-war" model was linearized, thus being limited to consider modest variations of the parameters around their nominal values. We considered on the anterior side a two-fold lower on-rate of force generators [19], resulting in half less engaged force generators than at the posterior, as previously reported [16]. We also assumed that this force is reduced by half after anaphase onset to account for sister chromatid separation [42]. We finally modelled the centering force by a spring according to [15] and the control parameter for advancing mitosis was the processivity [18]. In comparison to trajectories reported previously [15], we could reproduce the global kinematics of posterior displacement, with a slow displacement prior to anaphase

and an acceleration after (Fig. 5, black curve, S7A5). In particular, this accounts well for the final position of the posterior centrosome. On this basis, we aimed to validate this simulated model to explore the consequences on the final spindle position of including microtubule dynamics in the model.

The active region but not the force generator total number dictates the final position of the spindle.

Consistent with observations in *let-99(RNAi)* treated embryos (Fig 3A) and [22], the final position of the posterior centrosome was displaced anteriorly when the boundary of the posterior active crescent moved towards the anterior, provided that this region was large enough to initiate posterior displacement (Fig. S7B). This result contrasted with the original "tug-of-war" prediction that the larger the cortical forces, the more posterior the displacement. The asymmetry of cortical pulling forces causing the posterior displacement is due to a larger number of active force generators on the posterior side [16], initially assumed to reflect an asymmetric total number of generators and recently proposed to be due to an asymmetric on-rate [19]. The original model predicted a linear dependence between the number of active force generators and the final spindle position [15]. The extended "tug-of-war" model offered a reduced sensitivity to this number in comparison (Fig. S7CD, SI text § 2.2.3), consistent with the observed robustness of oscillation onset position (Fig. S6C). We attributed this robustness to a less pronounced increase of cortical pulling forces when the centrosome crossed the position of the boundary (Fig. S7A4). We concluded that accounting for the dynamics of microtubules is needed to correctly understand the mechanism setting the final position of the spindle, superseding the original "tug-of-war", and accounting for the dependence of the final spindle position on the cortical boundary rather than number of active force generators.

The robustness of spindle final position towards the final force generator processivity.

In the original "tug-of-war" model, the final spindle position was predicted to not only depend on the imbalance of force generator number or their on-rate, but also on their final processivity. This prediction is poorly consistent with the *such-1* mutant. In this experiment, which affected mitosis progression and thus likely final processivity, the final posterior centrosome position is not altered (Table 1) [23]. We observed that extended model can account for this robustness in modest final processivity variations (Fig. 5). We suggest that the extended model better recapitulates the robustness of the final spindle positioning to changes in force generator number or dynamics. This is essential to proper positioning of the cytokinesis furrow, in particular.

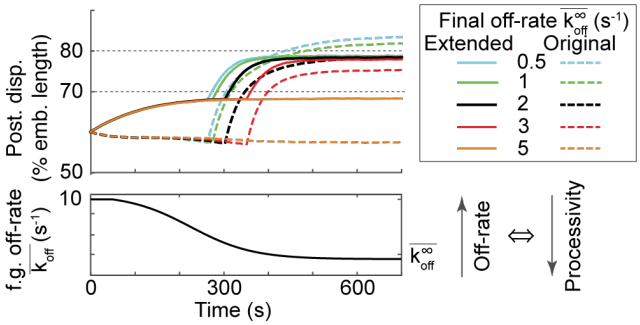

Figure 5: Extended model offers robustness to variation in final force generator processivity. Stochastic simulation of the displacement of the posterior centrosome, when varying the final force generator detachment rate (off-rate, inverse of the processivity), which is color coded. A typical case of its time evolution is represented in the bottom part. Earlier than 300 s, detachment rates are very close disregarding their final values, leading to superimposed posterior centrosome trajectory. The dashed line represents the result with the original model while the solid line corresponds to the extended model (SI text § 3). The dispersion of the final values in the original model revealed a lack of robustness to variation in final off-rate. Numerical parameters in use are reproduced in SI text § 4.

Discussion

By measuring the spatial distribution of microtubule contacts at the cell cortex, we found that they are modulated in space and more concentrated in the regions closer to the centrosomes. It is however noteworthy that the total number of contacts scale up (as seen in Fig. 1, 80 s after anaphase onset) due to the increased nucleation and persistence of microtubules, as expected from their regulation along the course of the mitosis [26]. This contact modulation regulates the forces responsible not only for the anaphase oscillations of the spindle but also for its posterior displacement. Interestingly, this causative force is under the control of the position of the posterior centrosome (the so called *positional switch*). These forces also contribute to spindle elongation and their positional regulation might create a link with tension-based spindle assembly checkpoint satisfaction [43]. We extended our previous "tug-of-war" model of spindle oscillations and posterior displacement [18] to account for this and validated it

experimentally. In particular, we observed that the position of oscillation onset, but not the timing, is robust to variations in embryo length, while also correlated to the size of the posterior active force generator region, putatively bounded by LET-99 [21, 22]. In the early stages of mitosis, the spindle lies in the middle of the embryo and both of the centrosomes are far from their respective cortex: thus, the imbalance in the number of active force generators [16] results in a slight posterior pulling force and causes a slow posterior displacement [17] (Fig. 2C, *left*). The closer the posterior centrosome gets to the cortex, the larger the force imbalance is, since more microtubules reach the cortex: the pulling force builds up more rapidly and the posterior displacement accelerates. The number of engaged force generators increases, exceeding the threshold for oscillation onset [18] (Fig. 2C, *middle*). Once the posterior centrosome crosses the boundary of the active region, the pulling forces start saturating because only their projection along the anteroposterior axis contributes (Fig. S2C, *right*): these forces, together with the centering forces [18], balance and set the position at which the posterior centrosome finally stops. They decide of the end–of–mitosis position of the spindle.

This proposed positional switch adds to the previously described temporal control via the processivity of force generators [18], in turn reflecting mitosis progression [23]. These two controls act independently, as they relate to two independent components. The *positional control* is determined by microtubule dynamics while the *temporal control* is set by the force generator dynamics. Indeed, the curve of the number of engaged force generators *versus* centrosome position (Fig. 2B) steeply increases from 60 % of embryo length because of microtubule dynamics, while this number saturates above 70 % due to force generator dynamics. Our model predicts respectively two necessary conditions for the oscillations to start (Figure 2D, blue curve): a large enough number of microtubules contacting the active region of the cortex, and a high enough processivity of force generators. Indeed, during anaphase, the temporal evolution of the amplitude of cortical pulling forces is controlled by the dynamics of force generators, as proposed previously, and as revealed by the timing of oscillation die down [18]. This dual control of pulling forces was furthermore confirmed by three experiments. Firstly, in *let-99(RNAi)* treated embryos, where the positional control is disturbed by displacing anteriorly the active region boundary; the final position of the centrosome is strongly altered (Fig. 3A) as predicted by the model (Fig. S7B), but the timing of oscillation die down is not significantly different from the control (Fig. 3B). Secondly, in *such-1(h1960)* mutants, where temporal control is perturbed via a delay in anaphase onset, the duration from anaphase onset to oscillation die down is the same as in the control, implying that die down timing is delayed in the same proportion as anaphase onset. In contrast, the positions of oscillation onset and die down are not altered by delaying anaphase onset (Table 1). Thirdly, we observed precocious oscillation die down upon decreasing the number of active force generators by a *gpr-2* null mutant (Fig. S6B); this number exceeds the threshold during a shorter time period, consistently with the original "tug-of-war" model prediction (see e.g. fig. 5C of [18]). Overall, these experiments support the conclusion that during anaphase, force generator dynamics dominate the control of anaphase oscillations.

We hypothesized that these combined controls, in particular the proposed positional switch, confer some robustness to the final position of the posterior centrosome and consequently of the spindle, for instance by buffering against variations in the initial positions of the centrosomes (Fig. S7E) or the final processivity that determines the final cortical pulling forces (Fig. 5). In terms of asymmetric cell division, the final position of the spindle contributes to prescribing the cytokinesis furrow position, which is essential to ensure correct partitioning of cell polarity cues and thus daughter cell fates [1-3]. Above the sole *C. elegans* nematode, we recently performed a comparative study between two nematode cousins (*C. elegans* and *C. briggsae*) [12]. We found in particular an alteration of cortical force generator regulation because of a duplication (GPR-1 and GPR-2) in *C. elegans* with respect to *C. briggsae* displaying only GPR-2 [12]. We proposed that this evolution was made possible by the positional switch and the robustness it creates towards force generator number or dynamics. Indeed, *C. briggsae* microtubule contacts at the cell cortex are modulated as in *C. elegans* (Fig. S3) and robustness to embryo length variations is also observed [12]. Interestingly, the positional control of anaphase oscillation onset in *C. briggsae* results in a 30 s delay between oscillation and anaphase onsets (attributed to spindle overcentation [12]), while the die down is synchronous with anaphase onset as predicted by our model. Furthermore, cross species insertion of GPR genes modulates oscillation amplitude but preserves the positional switch consistent with our *gpr-2(ok1179)* experiment. The robustness in final spindle positioning is likely true beyond these sole two species [44]. In conclusion, the proposed robustness mechanism has enabled changes in the regulation of nuclei/centrosome complex position during the course of evolution despite such regulation being essential.

At the core of this robustness mechanism is the dynamic instability of microtubules, and more precisely the dependency of the number of contacts on the distance from centrosome to cortex. Indeed, said distance is measured in "units of microtubule dynamics" (SI text § 2.1.2). This is a classic mechanism to create centering [28, 45] or other shape dependent mechanisms [29, 46, 47], although it was always inferred from cell level properties. In contrast, we measured here the distribution of the contacts localizing them directly at the cortex at the microscopic level and observed a density ratio of about 2 between the most and least microtubule–contact–dense regions for a given time. This ratio represents the sensitivity to centrosome position (SI text §2.1.2). From a theoretical point of view, considering the ellipsoidal shape of the *C. elegans* embryo and the measured microtubule dynamics (see above), the predicted maximal ratio is 1.64. Our experimental one is close to this latter value, suggesting that the microtubule dynamics parameters are optimal to create the positional control discussed here.

Conclusion

The study of the mechanism that leads to the precise timing and positioning of the transverse oscillation onset in the one-cell embryo of *C. elegans* has highlighted the key role of microtubule dynamics in probing the boundary of the active force generator region. This *positional control* of spindle rocking acts in complement to previously established regulation through pulling force machinery dynamics (*temporal control*). Both controls set independent switches preventing premature force burst and centrosome oscillations and leading to a robust mechanism of asymmetric cell division. Indeed, these spatial and temporal switches control not only the oscillation onset but also the final spindle position. The posterior centrosome position provides a feedback to the pulling forces causing the spindle displacement. As in the oscillation onset mechanism, microtubule dynamics contribute also to probing the cell shape and maintaining robustness in setting the final position of the posterior centrosome as a proportion of the AP axis. In particular, this final position is robust to changes in the final dynamics of force generators (processivity), putatively linked to the mitosis progression. This is a novel example of a microfilaments-based mechanical system providing robustness to perturbation. In this instance, changes of cortical pulling force level and timing, due to the evolution of essential genes GPR-1/2^{LGN} in its generating complex[12], was buffered through microtubule dynamics.

Author contributions

HB, LC, MD and JP designed the research and analyzed the data; HB, LC, SP and JP performed the research. HB and JP wrote the paper.

Acknowledgments

The *gpr-2(ok1179)* backcrossed 10x is a kind gift of Prof. A.A. Hyman. We thank Dr G. Michaux for feeding clones library and technical support. We also thank Drs B. Mercat, A. Pacquelet, X. Pinson, Y. Le Cunff, D. Fairbrass, G. Michaux, R. Le Borgne, S. Huet, F. Argoul and A. Arnéodo for technical help, critical comments on the manuscript and discussions about the project. JP was supported by a CNRS ATIP starting grant and *la ligue nationale contre le cancer*. Some strains were provided by the CGC, which is funded by NIH Office of Research Infrastructure Programs (P40 OD010440; University of Minnesota, USA). Microscopy imaging was performed at the MRIC facility, UMS 3480 CNRS / US 18 INSERM / Univ. Rennes 1. Spinning disk was co-funded by CNRS, *Rennes métropole* and *region Bretagne* (grant AniDyn-MT), which also funded H.B. fellowship. H.B also acknowledges EMBO for her long term post-doctoral fellowship.

Material and Methods

Culturing C. elegans

C. elegans nematodes were cultured as described in [48] and dissected to obtain embryos. The strains were maintained at 25°C and imaged at 23°C, except *gpr-2* mutant, *such-1* mutant and their controls, which were maintained at 15°C and imaged at 18°C. The strains were handled on nematode medium plates and fed with OP50 bacteria.

Strains

The TH65 *C. elegans* (*Ce*) YFP::TBA-2 (α-tubulin) [26] and ANA020 *C. briggsae* (*Cb*) GFP::β-tubulin strains (fluorescent labelling of microtubules) were used as the standards for the "landing assay." TH27 *C. elegans* GFP::TBG-1 (γ-tubulin) [49] and *C. briggsae* ANA022 TBG-1::GFP [12] strains (fluorescent labelling of the centrosomes) were the standard used for the "centrosome tracking assay." *C. elegans* TH231 SPD-2::GFP strain with centrosome labelling crossed to OD56 mCherry::HIS-58 histone labelling was the control used for timing the events (table 1). It was crossed with the KR4012 *such-1(h1960)* mutant strain [32] to create JEP16. Centrosome tracking upon mutating *gpr-2* was performed on JEP14 strain obtained by crossing the TH291 *gpr-2*(*ok1179*) backcrossed 10 times strain and TH27 *C. elegans* GFP::TBG-1 (γ-tubulin).

Gene inactivation by use of mutants or protein depletion by RNAi feeding

RNAi experiments were performed by ingestion of transformed HT115 bacteria. let99, cid1 and c27d9.1 genes were amplified from AF16 genomic ADN and cloned into the L4440 plasmid. The feeding during 48h (except for let-99, reduced to 16-24h) was performed at 20°C to obtain stronger phenotypes. The control embryos for the RNAi experiments were treated with bacteria carrying the empty plasmid L4440.

Embryos preparation for imaging

Embryos were dissected in M9 buffer and mounted on a 2% w/v agarose, 0.6 % w/v NaCl and 4 % w/v sucrose pad, between a slide and a coverslip and were observed on different microscopic setups depending on the assays. We confirmed that embryos were devoid from phototoxicity and photodamage by checking that the rate of subsequent divisions was normal [50]. Fluorescent lines were imaged at 23°C unless stated otherwise.

Imaging of microtubule contacts at the cortex

Embryos were dissected in M9 buffer and mounted on a 2% w/v agarose, 0.6 % w/v NaCl and 4 % w/v sucrose pad. We imaged *C. elegans* or *C. briggsae* one–cell embryos at the cortex plane in contact with the glass slide (Figure S1A) from the nuclear envelop breakdown (NEBD) until the end of the cell division. In particular, we aimed to preserve embryo shape at most. Thus, the thickness of the perivitelline space [51] required the use of spinning disk microscopy rather than TIRF (Fig. S1A). Therefore, cortical microtubule contact tracking was performed on a LEICA DMI6000 / Yokogawa CSU-X1 M1 spinning disc microscope, using HCX Plan Apo. 100x/NA 1.4 Oil. Illumination was performed by a white light Fianium laser filtered around 514 nm by a homemade setup. To account for the fast dynamics of the microtubules at the cortex, images were acquired with a 100 ms exposure time (10 Hz) using an ultra-sensitive EMCCD Roper instrument evolve camera and the Metamorph software (Universal imaging Corp.) without binning. We kept the embryos at 23°C during the experiments. To image embryos at the cortex we moved the focus typically between 12 to 15 μm below the spindle plane (Fig. S1A).

Imaging the centrosomes

For the "centrosome tracking" and the "events timing" assays, embryos were observed at the mid-plane using a Zeiss AxioImager upright microscope modified for long-term time-lapse. Firstly, an extra anti-heat filter was added on the mercury lamp light path. Secondly, to decrease the bleaching and obtain optimal excitation, we used an enhanced transmission 12 nm band-pass excitation filter centered on 485 nm (AHF analysentechnik, Tübingen, Germany). We used a 100x/NA 1.45 Oil plan-Apo objective. Images were acquired with an Andor Ixon3 EMCCD 512x512 camera at 33 frames per second and using the Solis software. We aligned centrosome tracks of individual embryos on the beginning of the spindle abrupt elongation (Fig. S8A) as an accurate landmark of anaphase onset [15] to average them or overlay them to "landing assay."

Statistics

Averaged values were compared using 2 tailed Student t-test with correction for unequal variance except otherwise stated. For sake of simplicity, we encoded confidence level using stars: * meaning $p \leq 0.05$, ** $p \leq 0.005$, *** $p \leq 0.0005$, **** $p \leq 0.00005$ and n.s. (for non-significant) meaning $p > 0.05$. n.s. indication might be omitted for sake of clarity. We abbreviated standard deviation by S.D., standard error by s.e. and standard error of the mean by s.e.m.

Data processing, Modelling and Simulation

All data analysis were developed using Matlab (The Mathworks). Modelling was performed using formal calculus software Mathematica (Wolfram). Numerical simulations were performed using simulink and matlab (The Mathworks).

Bibliography

1. Betschinger, J., and Knoblich, J.A. (2004). Dare to be different: asymmetric cell division in Drosophila, C. elegans and vertebrates. Curr Biol *14*, R674-685.
2. Gillies, T.E., and Cabernard, C. (2011). Cell division orientation in animals. Curr Biol *21*, R599-609.
3. White, E.A., and Glotzer, M. (2012). Centralspindlin: At the heart of cytokinesis. Cytoskeleton (Hoboken) *69*, 882-892.
4. Rappaport, R. (1971). Cytokinesis in animal cells. Int Rev Cytol *31*, 169-213.
5. Knoblich, J.A. (2010). Asymmetric cell division: recent developments and their implications for tumour biology. Nat Rev Mol Cell Biol *11*, 849-860.
6. Morin, X., and Bellaiche, Y. (2011). Mitotic spindle orientation in asymmetric and symmetric cell divisions during animal development. Dev Cell *21*, 102-119.
7. Gonczy, P. (2008). Mechanisms of asymmetric cell division: flies and worms pave the way. Nat Rev Mol Cell Biol *9*, 355-366.
8. McNally, F.J. (2013). Mechanisms of spindle positioning. J. Cell Biol. *200*, 131-140.
9. Nguyen-Ngoc, T., Afshar, K., and Gonczy, P (2007). Coupling of cortical dynein and G alpha proteins mediates spindle positioning in Caenorhabditis elegans. Nat. Cell Biol. 9 *1294-1302*.
10. Colombo, K., Grill, S.W., Kimple, R.J., Willard, F.S., Siderovski, D.P., and Gonczy, P. (2003). Translation of polarity cues into asymmetric spindle positioning in Caenorhabditis elegans embryos. Science *300*, 1957-1961.
11. Park, D.H., and Rose, L.S. (2008). Dynamic localization of LIN-5 and GPR-1/2 to cortical force generation domains during spindle positioning. Dev. Biol. *315*, 42-54.
12. Riche, S., Zouak, M., Argoul, F., Arneodo, A., Pecreaux, J., and Delattre, M. (2013). Evolutionary comparisons reveal a positional switch for spindle pole oscillations in Caenorhabditis embryos. J Cell Biol *201*, 653-662.
13. Ahringer, J. (2003). Control of cell polarity and mitotic spindle positioning in animal cells. Curr. Opin. Cell Biol. *15*, 73-81.
14. Kimura, A., and Onami, S. (2007). Local cortical pulling-force repression switches centrosomal centration and posterior displacement in C. elegans. J Cell Biol *179*, 1347-1354.
15. Pecreaux, J., Redemann, S., Alayan, Z., Mercat, B., Pastezeur, S., Garzon-Coral, C., Hyman, A.A., and Howard, J. (2016). The Mitotic Spindle in the One-Cell C. elegans Embryo Is Positioned with High Precision and Stability. Biophys J *111*, 1773-1784.
16. Grill, S.W., Howard, J., Schaffer, E., Stelzer, E.H., and Hyman, A.A. (2003). The distribution of active force generators controls mitotic spindle position. Science *301*, 518-521.
17. Labbe, J.C., McCarthy, E.K., and Goldstein, B. (2004). The forces that position a mitotic spindle asymmetrically are tethered until after the time of spindle assembly. J Cell Biol *167*, 245-256.
18. Pecreaux, J., Roper, J.C., Kruse, K., Julicher, F., Hyman, A.A., Grill, S.W., and Howard, J. (2006). Spindle oscillations during asymmetric cell division require a threshold number of active cortical force generators. Curr. Biol. *16*, 2111-2122.
19. Rodriguez Garcia, R., Chesneau, L., Pastezeur, S., Roul, J., Tramier, M., and Pecreaux, J. (submitted). Dynamics of dynein at microtubule plus-ends and the cortex during the division of the C. elegans zygote. Nature communications.
20. Grill, S.W., Gonczy, P., Stelzer, E.H., and Hyman, A.A. (2001). Polarity controls forces governing asymmetric spindle positioning in the Caenorhabditis elegans embryo. Nature *409*, 630-633.
21. Wu, J.C., and Rose, L.S. (2007). PAR-3 and PAR-1 inhibit LET-99 localization to generate a cortical band important for spindle positioning in Caenorhabditis elegans embryos. Mol Biol Cell *18*, 4470-4482.
22. Krueger, L.E., Wu, J.C., Tsou, M.F., and Rose, L.S. (2010). LET-99 inhibits lateral posterior pulling forces during asymmetric spindle elongation in C. elegans embryos. J Cell Biol *189*, 481-495.

23. McCarthy Campbell, E.K., Werts, A.D., and Goldstein, B. (2009). A cell cycle timer for asymmetric spindle positioning. PLoS Biol *7*, e1000088.
24. Labbe, J.C., Maddox, P.S., Salmon, E.D., and Goldstein, B. (2003). PAR proteins regulate microtubule dynamics at the cell cortex in C. elegans. Curr Biol *13*, 707-714.
25. Kozlowski, C., Srayko, M., and Nedelec, F. (2007). Cortical microtubule contacts position the spindle in C. elegans embryos. Cell *129*, 499-510.
26. Srayko, M., Kaya, A., Stamford, J., and Hyman, A.A. (2005). Identification and characterization of factors required for microtubule growth and nucleation in the early C. elegans embryo. Dev Cell *9*, 223-236.
27. Dogterom, M., and Yurke, B. (1998). Microtubule dynamics and the positioning of microtubule organizing centers. Physical Review Letters *81*, 485-488.
28. Dogterom, M., Kerssemakers, J.W., Romet-Lemonne, G., and Janson, M.E. (2005). Force generation by dynamic microtubules. Curr Opin Cell Biol *17*, 67-74.
29. Minc, N., Burgess, D., and Chang, F. (2011). Influence of cell geometry on division-plane positioning. Cell *144*, 414-426.
30. Thery, M., Jimenez-Dalmaroni, A., Racine, V., Bornens, M., and Julicher, F. (2007). Experimental and theoretical study of mitotic spindle orientation. Nature *447*, 493-496.
31. Tsou, M.F., Ku, W., Hayashi, A., and Rose, L.S. (2003). PAR-dependent and geometry-dependent mechanisms of spindle positioning. J Cell Biol *160*, 845-855.
32. Tarailo, M., Kitagawa, R., and Rose, A.M. (2007). Suppressors of spindle checkpoint defect (such) mutants identify new mdf-1/MAD1 interactors in Caenorhabditis elegans. Genetics *175*, 1665-1679.
33. Mitchison, T., and Kirschner, M. (1984). Dynamic instability of microtubule growth. Nature *312*, 237-242.
34. Howard, J. (2006). Elastic and damping forces generated by confined arrays of dynamic microtubules. Phys Biol *3*, 54-66.
35. O'Rourke, S.M., Christensen, S.N., and Bowerman, B. (2010). Caenorhabditis elegans EFA-6 limits microtubule growth at the cell cortex. Nat Cell Biol *12*, 1235-1241.
36. O'Toole, E.T., McDonald, K.L., Mantler, J., McIntosh, J.R., Hyman, A.A., and Muller-Reichert, T. (2003). Morphologically distinct microtubule ends in the mitotic centrosome of Caenorhabditis elegans. J Cell Biol *163*, 451-456.
37. Edwards, J. (1892). An elementary treatise on the differential calculus, with applications and numerous examples, (London, New York,: Macmillan).
38. Grill, S.W., Kruse, K., and Julicher, F. (2005). Theory of mitotic spindle oscillations. Physical Review Letters *94*, 108104.
39. Koonce, M.P., and Tikhonenko, I. (2012). Dynein Motor Mechanisms. In Dyneins : structure, biology and disease, 1st Edition, S.M. King, ed. (Amsterdam ; Boston: Academic Press), pp. xv, 639 p.
40. Garzon-Coral, C., Fantana, H.A., and Howard, J. (2016). A force-generating machinery maintains the spindle at the cell center during mitosis. Science *352*, 1124-1127.
41. Hosea, M.E., and Shampine, L.F. (1996). Analysis and implementation of TR-BDF2. Applied Numerical Mathematics *20*, 21-37.
42. Mercat, B., Pinson, X., Le Cunff, Y., Fouchard, J., Mary, H., Pastezeur, S., Gachet, Y., Tournier, S., Bouvrais, H., and Pecreaux, J. (in preparation). Micro-fluctuations of spindle length reveal its dynamics over cell division.
43. Cimini, D., Wan, X., Hirel, C.B., and Salmon, E.D. (2006). Aurora kinase promotes turnover of kinetochore microtubules to reduce chromosome segregation errors. Curr Biol *16*, 1711-1718.
44. Farhadifar, R., Baer, C.F., Valfort, A.C., Andersen, E.C., Muller-Reichert, T., Delattre, M., and Needleman, D.J. (2015). Scaling, selection, and evolutionary dynamics of the mitotic spindle. Curr Biol *25*, 732-740.
45. Wuhr, M., Dumont, S., Groen, A.C., Needleman, D.J., and Mitchison, T.J. (2009). How does a millimeter-sized cell find its center? Cell Cycle *8*, 1115-1121.
46. Daga, R.R., and Nurse, P. (2008). Interphase microtubule bundles use global cell shape to guide spindle alignment in fission yeast. J Cell Sci *121*, 1973-1980.
47. Thery, M. (2010). Micropatterning as a tool to decipher cell morphogenesis and functions. J Cell Sci *123*, 4201-4213.
48. Brenner, S. (1974). The genetics of Caenorhabditis elegans. Genetics *77*, 71-94.
49. Oegema, K., Desai, A., Rybina, S., Kirkham, M., and Hyman, A.A. (2001). Functional analysis of kinetochore assembly in Caenorhabditis elegans. The Journal of Cell Biology *153*, 1209-1226.
50. Riddle, D.L. (1997). C. elegans II, (Plainview, N.Y.: Cold Spring Harbor Laboratory Press).

51. Olson, S.K., Greenan, G., Desai, A., Muller-Reichert, T., and Oegema, K. (2012). Hierarchical assembly of the eggshell and permeability barrier in C. elegans. J Cell Biol *198*, 731-748.

Supplementary Figures

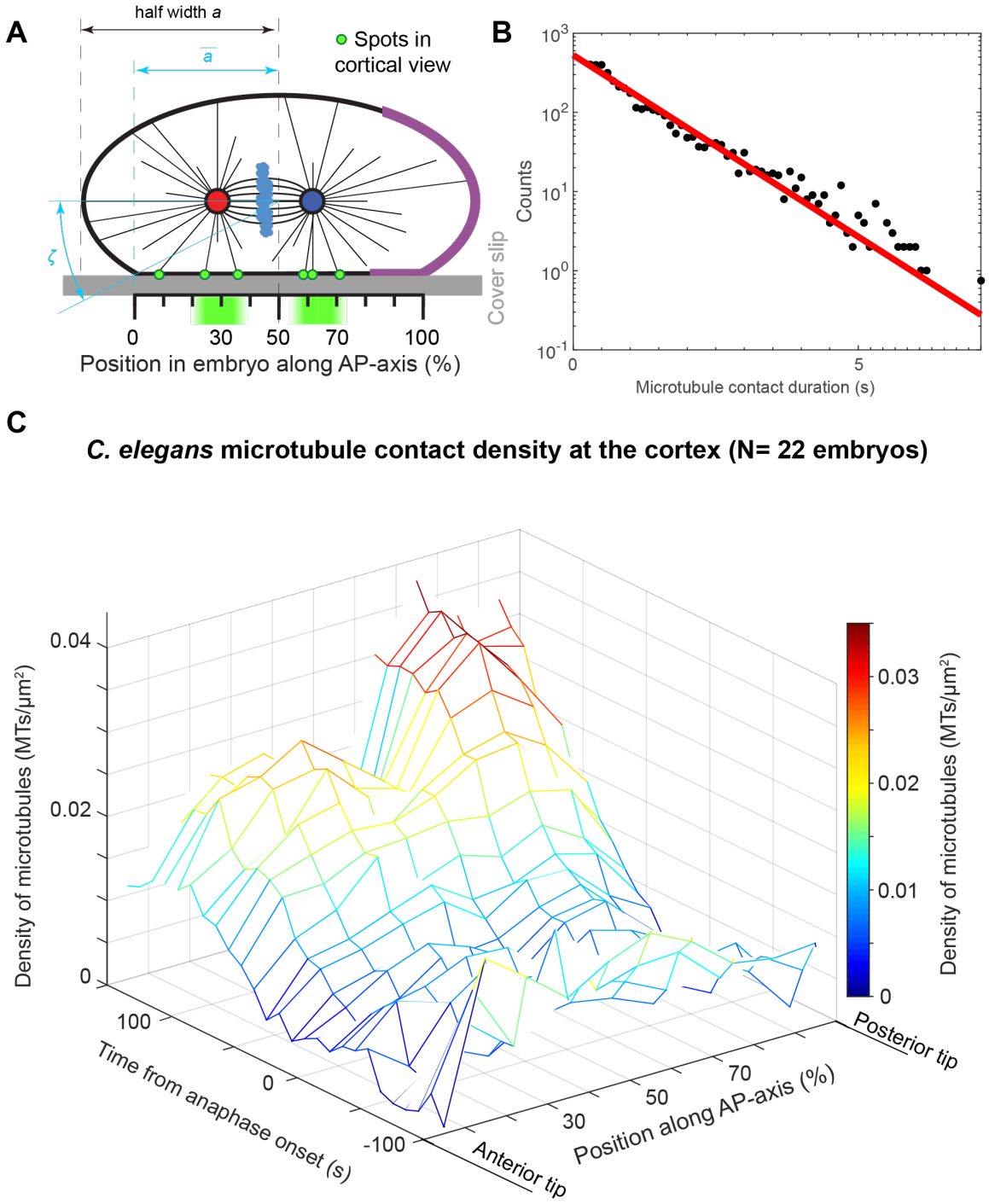

Figure S1: Microtubule contact density at the cell cortex in *C. elegans*.

(**A**) Experimental setup to image microtubule contacts density at the cell cortex. Gray rectangle at bottom represents the cover-slip, above it, the green dots depict the detected spots. Below it, the scale represents the 10 regions along the anteroposterior axis used for analysis (see Methods). Red and blue disks correspond to the anterior and posterior centrosomes, respectively. Light blue clouds represent the chromosomes. Microtubules emanating from the centrosomes are depicted by thin black lines. Purple cortical region corresponds to the posterior crescent, where lie the active force generators. (**B**) Histogram, in log–linear axes, of the measured residency times during metaphase and anaphase for a single embryo (black dots), fitted with an exponential (red line) 0.95 ± 0.03 s as decay time (N=3832 MTs) (**C**) Microtubule contacts density at the cortex obtained by analyzing spinning disk microcopy images of YFP::α-tubulin strain (see Methods) (N=22 *C. elegans* embryos). Data are the same as in Fig. 1. Time was indicated from anaphase onset.

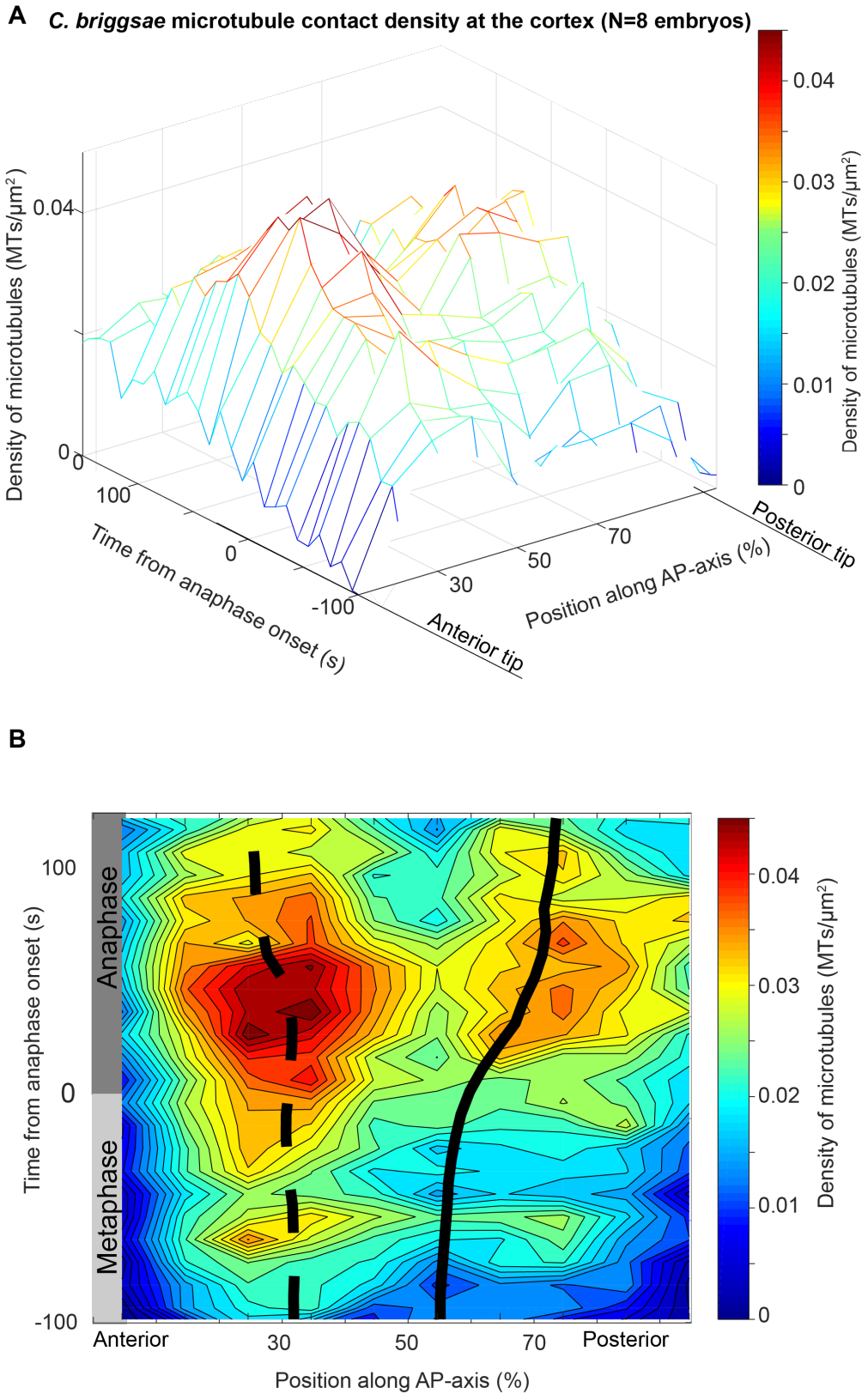

Figure S2: Microtubule contact density at the cell cortex in *C. briggsae*.
(**A**) Microtubule contacts density at the cortex obtained by analyzing spinning disk microcopy images of GFP::β-tubulin strain (see Methods), averaged along the transverse axis *versus* time and position along the antero-posterior axis (N=7 *C. briggsae* embryos). (**B**) The same microtubule contacts density represented by a heat map. The centrosome trajectories, obtained by imaging the γ-tubulin::GFP strain in the spindle plane, were superimposed (N=8 embryos). Dashed line represents the anterior centrosome trajectory, solid line the posterior. Times were reported from anaphase onset.

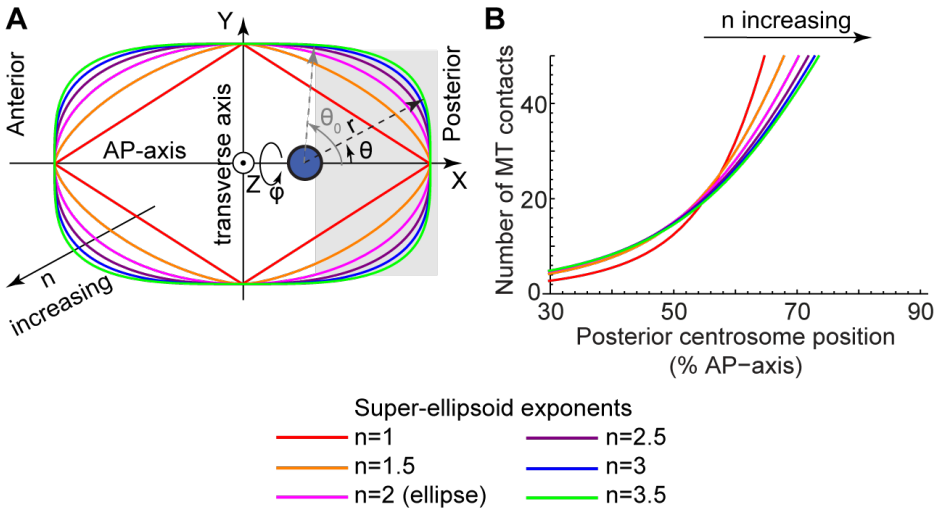

Figure S3: Modelling embryo shape by super-ellipsoids of various exponents preserves the switch-like behavior of the number of microtubules contacting the cortex in the active region upon centrosome displacement towards the posterior. Embryo was modelled by a super-ellipsoid of exponent n (long axis 24.6 µm and short axis 15.75 µm, SI text § 2.2.3). $n=2$ corresponds to the ellipse. **(A)** super-ellipses with exponent n from 1 to 3.5. The centrosome was positioned at 67 % of the AP-axis and denoted by a blue disk. Cartesian axes (X,Y,Z) are indicated as well as spherical coordinates centered on the centrosome (r,θ,ϕ). The boundary of the active region was set to 70 % of embryo length and depicted by a gray rectangle. Its boundary is at angle θ_0 in centrosome-centered spherical coordinates **(B)** Number of microtubules contacting the active region *versus* the position of the posterior centrosome along the AP axis, in % of embryo length, for the super-ellipsoids of revolution based on super-ellipses plotted in panel A. Numerical parameters in use are reproduced in SI text § 4.

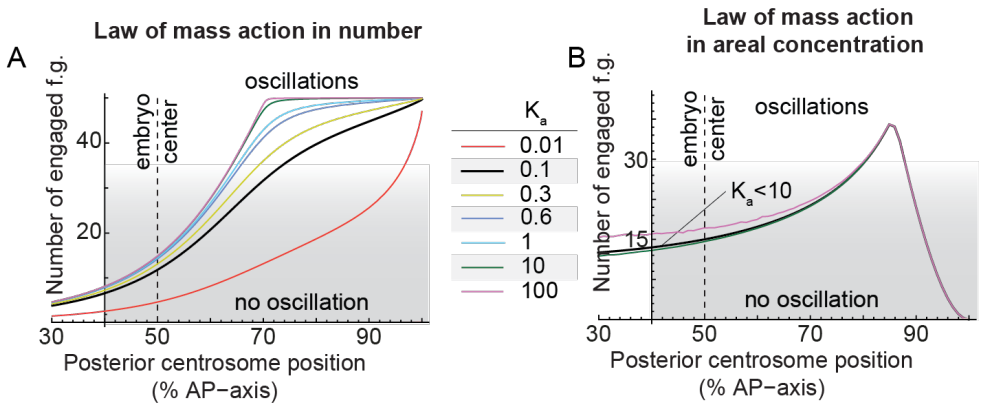

Figure S4: Comparison of model using law of mass action in number or in areal concentration. Number of engaged force generators (f.g.), i.e. pulling on a microtubule, *versus* the posterior displacement of the centrosome along the AP-axis varying the force-generator–microtubule association constant K_a (SI text § 2.2.2). For the centrosome position above 60 % of the AP axis, the number of engaged force generators steeply increased and saturated above 70 %, creating a switch–like behavior. Force-generator–microtubule binding was modelled by the law of mass action in: **(A)** number, with total number of force generators N=50 or **(B)** areal concentration (see section § 2.2.2), with N=500 to get similar number of engaged force generators in both cases and a value consistent with experimental estimate between 10 and 100 (Grill et al., 2003) (SI text § 2.2.4). Numerical parameters in use are reproduced in SI text § 4. Gray shading depicts conditions where the number of engaged force generators was too low to permit oscillations (below threshold).

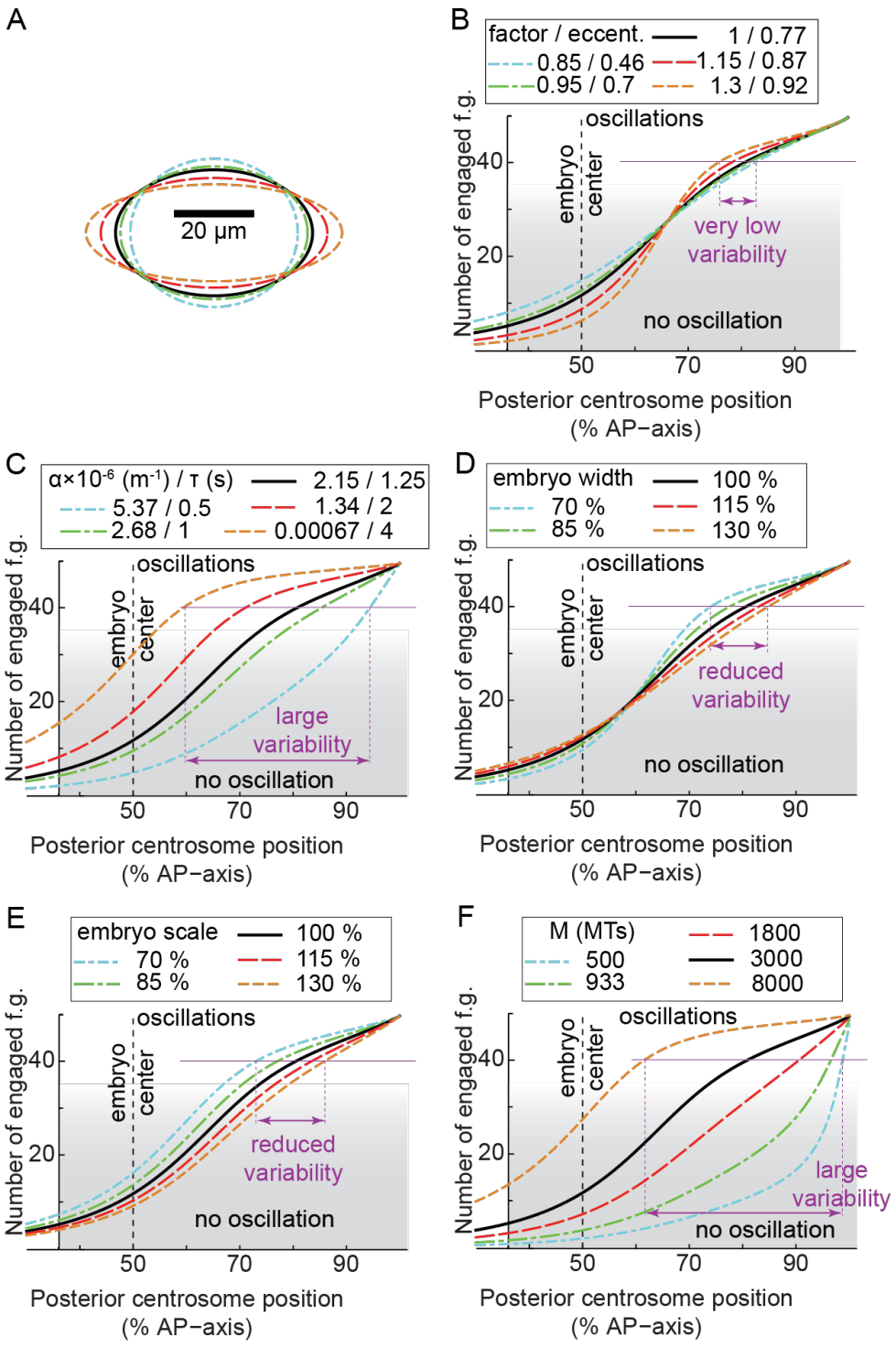

Figure S5: Sensitivity analysis of the extended "tug-of-war" model for oscillation onset. Number of engaged force generators (f.g.), i.e. pulling on a microtubule, *versus* the posterior displacement of the centrosome along the AP-axis varying: **(B)** the eccentricity of the ellipse (shapes reproduced in panel **A**) modelling the embryo by scaling its length by a factor and the width inversely; **(C)** the dynamics of the microtubules summarized by parameter α in m^{-1} and its equivalent cortical residency time τ in s, assuming growing and shrinking rates remain constant (SI text § 2.1.2); **(D)** embryo width expressed in % of control value; **(E)** embryo scale factor on length and width (keeping proportions); and **(F)** the total number of microtubules emanating from a single centrosome. In all cases, black lines correspond to value in control conditions, cold colors to lower values and hot colors to higher values. Numerical parameters in use are reproduced in SI text § 4. Gray shading depicts conditions where the number of engaged force generators was too low to permit oscillations (below threshold). Purple thin lines, of equal length in each panel, gives a scale of variability close to the threshold number of force generators enabling oscillations.

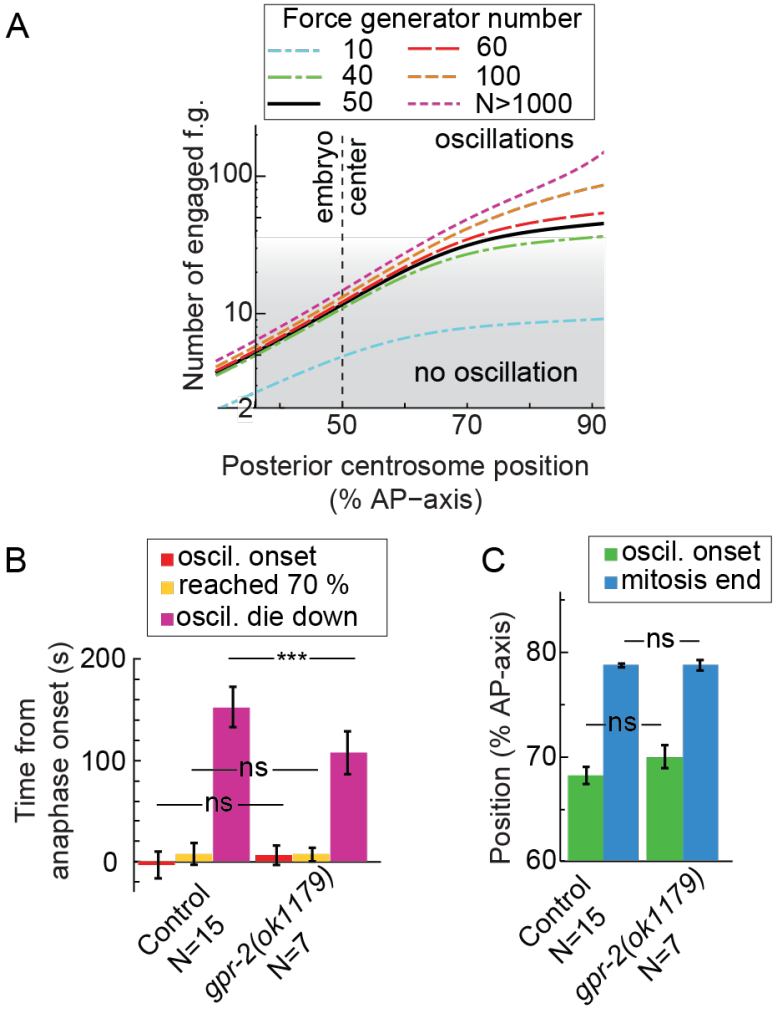

Figure S6: Force generator amount does not contribute to setting the position switch. (A) Modelled number of microtubules (MTs) contacting the posterior crescent (active region) of the cortex *versus* the posterior displacement of the centrosome along the AP-axis in % of embryo length. The number of force generators available was encoded by the color of the lines, with black line corresponding to unperturbed embryo and green curve to *gpr-2(ok1179)* mutant. Numerical parameters in use are reproduced in SI text § 4. Gray shading depicts conditions where the number of engaged force generators was too low to permit oscillations (below threshold). **(B)** Timings of oscillation onset, die down, and posterior centrosome reaching 70 % of embryo length and **(C)** positions of oscillation onset and die down upon depletion of active force generators. We measured GFP::γ-tubulin embryos either crossed to *gpr-2(ok1179)* (N=7) or N=15 control ones at 18ºC. Error bars indicate SD and stars indicate significant differences (see methods).

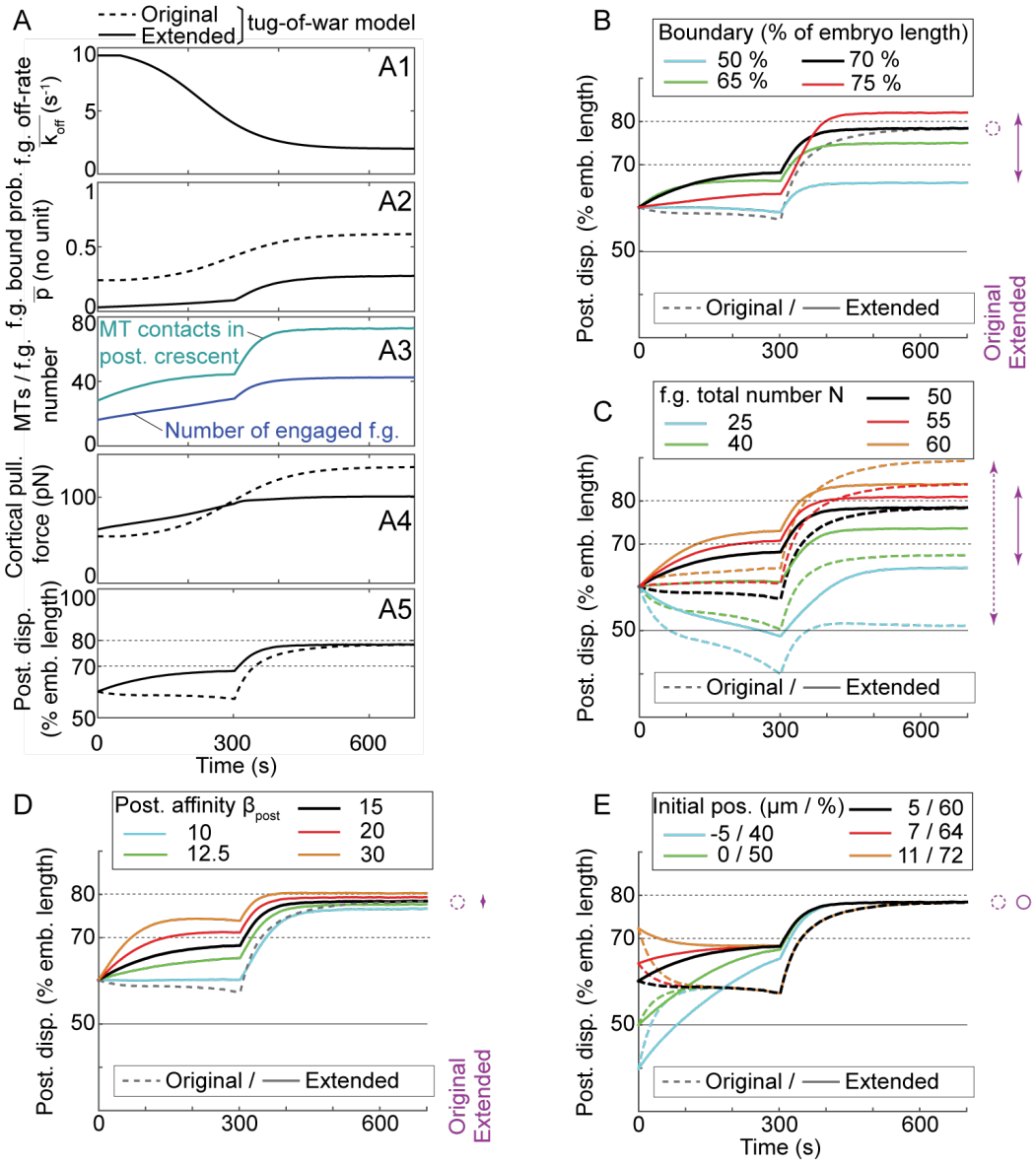

Figure S7: Extended model final position sensitivity analysis. Stochastic simulations of the displacement of the posterior centrosome. Dashed lines represent the results with the original model while solid lines correspond to extended model (SI text § 3). **(A)** Typical run showing from top to bottom: (A1) the force generator detachment rate, which is the control parameter encoding the progression through the mitosis (Pecreaux et al., 2006); (A2) the probability $\overline{p}$ for a force generator to be bound; (A3) the number of astral microtubules contacting the cortex in the posterior crescent (green line) and the number of engaged force generators in this same region (blue line) both for the extended model; (A4) the cortical force exerted by these force generators on the posterior centrosome; (A5) and the posterior displacement obtained consequently. **(B-F)** Posterior displacement averaged over 25 simulation runs varying respectively: (B) the boundary of the posterior crescent (active region) in % of embryo length; (C) the total force generator number available per half embryo; (D) the force generator attachment rate (on-rate) pre-factor β on posterior (asymmetry of β encodes the polarity, see SI text § 3 after Rodriguez Garcia et al. 2017); (E) and the initial position of the centrosome. Grey dashed line corresponds to original model when it does not depend on the parameter considered. In all cases, the value of the parameters are color coded: black line corresponds to value in control conditions, cold colors to lower values and hot colors to higher values. The dispersions of the final values for each case are represented by purple arrows (dashed for original model and solid for extended model); a larger span reveals a lack of robustness to variation of the parameter in the plot. A circle is used when the parameter has no effect on the final value. Numerical parameters in use are reproduced in SI text § 4.

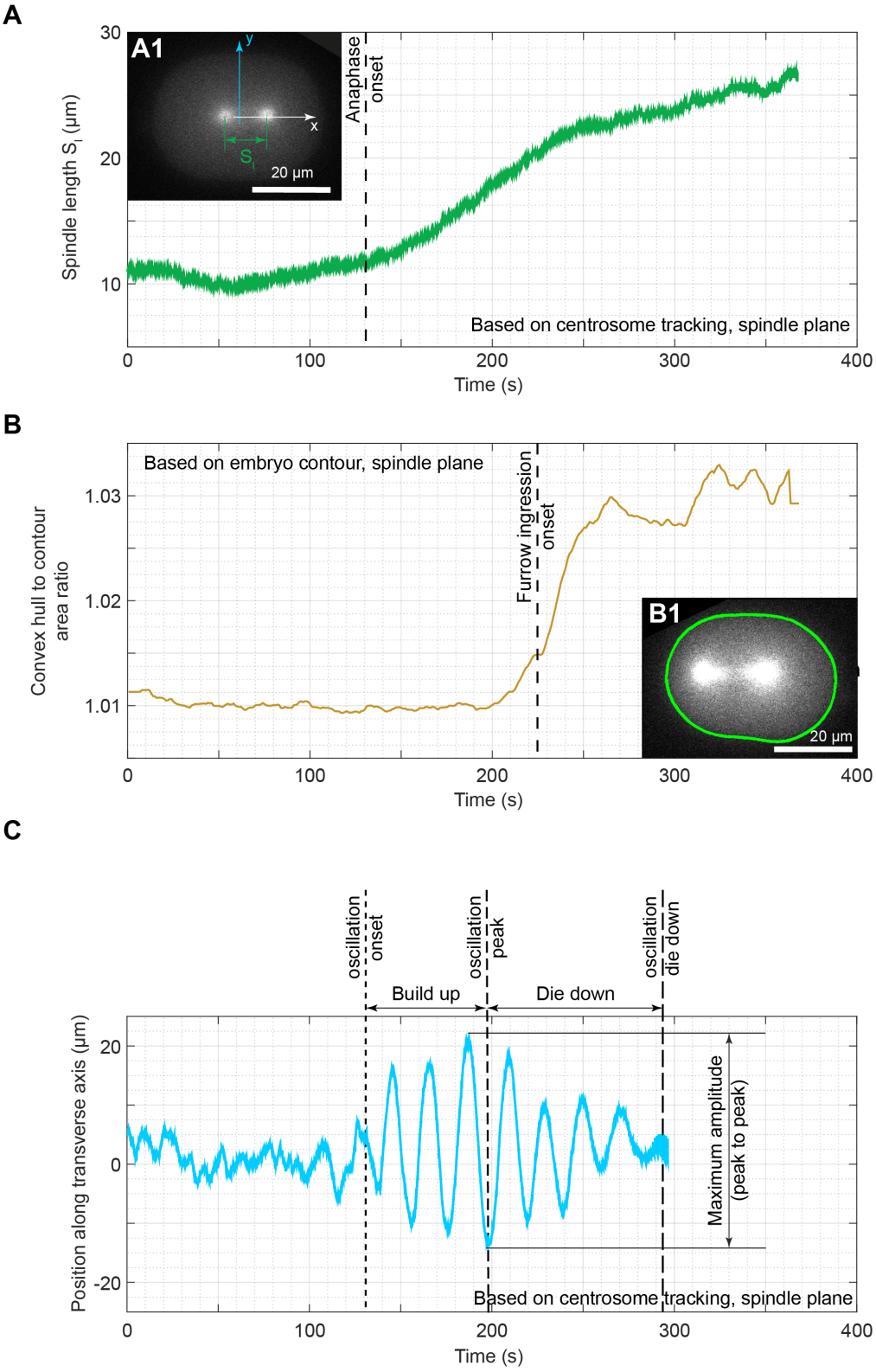

Figure S8: Landmarks used to set reference times and oscillation characteristics.
C. elegans centrosome trajectories and embryo shape were measured in the spindle plane imaging α-tubulin::YFP strain (inset **A1)**. (**A**) The spindle length was measured as the distance between the two centrosomes. Anaphase onset was defined as the inflexion point towards a steeper increase of the length and denoted by a vertical dashed line. (**B**) Ratio of convex contour to active contour are related to the convexity of the embryo contour (see Suppl. Expe. Proc., inset **B1**) and plotted along time. The furrow ingression timing is set as the inflection in ratio steep increase and denoted by the vertical dashed line. (**C**) Position of the posterior centrosome along the transverse axis of the embryo. The timings for the oscillation onset, peak amplitude and disappearance are denoted by small, mid-sized and long dashed vertical lines, respectively. Vertical arrow indicates the measurement of maximum amplitude (peak to peak distance in consecutive extrema).

Supplementary Experimental procedures

"Landing assay": Pipeline to measure microtubule contact density and dynamics at the cortex

Motivation for the strain choice

We used nematode strains, where the whole microtubules were labelled using yfp::α-tubulin and gfp::tubulin transgenes for *C. elegans* and *C. briggsae* embryos, respectively, rather than a labelling of the +TIPs of the microtubule via the EB homolog proteins. The advantage was twofold: (1) this labelling preserved the dynamics of the microtubules unlike the overexpression of EB proteins (Straube and Merdes 2007, Komarova, De Groot et al. 2009), and (2) this labelling enabled us to measure the duration of the residency of microtubules themselves at the cortex, not only the time spent growing there, which substantially differs (Kozlowski, Srayko et al. 2007). We compensated the low SNR present within the biological images by tracking with u-track software (Jaqaman, Loerke et al. 2008) to gain a robust detection of microtubule contacts and computed density from tracks.

Preprocessing of the cortical images

Since microtubule tubulin spot signal was very weak at the cortex, we denoised the images to increase the signal-to-noise ratio. Such a denoising usually relies on the assumption that the noise is non-correlated in space and time and follows a Gaussian or Poisson distribution. We opted for the kalman filtering/denoising (Kalman 1960). To perform Kalman denoising, we applied the following parameters: the gain was set at 0.5 and the initial estimate of the noise was equal to 0.05.

Automated tracking of YFP::α-tubulin fluorescent spots at the cortex

Because a large number of tracks was present at the cortex, we sought an algorithm with robust linking. We opted for u-track (Jaqaman, Loerke et al. 2008) with parameters reproduced in table below. We validated these parameters by analyzing fabricated images of known dynamics (see simulation section below), found good colocalization between prescribed tracks in simulation and recovered ones, and measured similar lifetimes of the recovered track durations to the prescribed ones. Because we were conservative in parametrizing u-track algorithm, it is possible that we missed some of the tracks that were displaying low fluorescent intensities.

Detection	
Gaussian standard deviation	1.4
Alpha-value for initial detection of local maxima	0.08
Rolling window time-averaging	3
Iterative Gaussian mixture-model fitting	0
Tracking	
Maximum gap to close	5
Merge split	0
Minimum length of track segments from first step	3
Cost function frame-to-frame linking	
Flag for linear motion	1
Allow instantaneous direction reversal	1

Search radius lower limit	1
Search radius upper limit	3
Standard deviation multiplication factor	3
Nearest neighbor distance calculation	1
Number of frames for nearest neighbor distance calculation	4
Cost function close gaps	
Flag for linear motion	1
Search radius lower limit	1
Search radius upper limit	3
Standard deviation multiplication factor	3
Nearest neighbor distance calculation	
Number of frames for nearest neighbor	4
Penalty for increasing gap length	1.5
Maximum angle between linear tracks segments	30

Measuring microtubule residency time at the cortex

We computed the histogram of the track durations of microtubule contacts at the cortex. We used a bin size of 100 ms, equal to acquisition time. The exponential fit of this histogram led to microtubule lifetime of about 1 s (Figure S1B), consistent with (Kozlowski, Srayko et al. 2007).

Computing microtubule contact density at the cortex

The "landing assay" consisted in measuring the cortical microtubule contacts (Figure S1A) during the different phases of the mitosis. The region of the embryo contacting the cover-slip was divided in ten regions of equal width along its long axis (AP-axis). The *uTrack* algorithm enabled us to follow frame after frame the microtubule contacts at the cortex and to have access to their trajectories (Jaqaman, Loerke et al. 2008). We segmented the embryo cytoplasm to follow changes in the shape of the embryo along the cell division using active contours (Pecreaux, Zimmer et al. 2006) and obtained the evolutions of the length and the area of the embryo during the mitosis. We could then count the number of microtubules contacting the cortex in the ten regions along the embryo length (Fig. S1A). To increase certainty on the results, the distribution of the microtubule contacts was averaged along time over 10 s. Finally, we used the onset of cytokinesis furrow ingression as a time reference to align the different microtubule cortical contact density map and then averaged over the embryos to get the final averaged density map.

Timing of furrow ingression onset and overlay assay

We first aimed to get the timing of cytokinesis furrow ingression onset, in both planes, by detecting the contour of the embryo taking advantage of the dye cytoplasmic fraction. We obtained the contour of the embryo using active contours (Pecreaux, Zimmer et al. 2006). We then set the onset of cytokinesis furrow ingression as the fast increase in embryo shape convexity (ratio of the convex area to active contour area, Fig. S8B), practically when it grew above 1.012. In the mid-plane, we calibrated the average time between anaphase, obtained from the inflexion in spindle elongation (Pecreaux, Redemann et al. 2016), and cytokinesis furrow ingression onset in the mid-plane. We then used it to estimate the anaphase onset from the measuring of furrow ingression onset at the cortex and to match the times in landing and centrosome tracking assays when plotting the overlay (Fig. 1 e.g.).

Robustness plot (fig. 4)

To assess the robustness of the position and timing at witch the posterior centrosome starts oscillating, and the position of oscillation die–down with respect to variations in embryo length, we aimed to use dimensionless

quantities. To do so for the timing, we used the reference duration T equal to the delay between two mitosis events independent of cell mechanics. We chose the nuclear envelope breakdown and the anaphase onset. For each experiment, we computed the shift of oscillation onset time with respect to anaphase onset time, t_o. Thus, the normalized shift $\overline{\delta t_o}$ is obtained by subtracting from the current value t_o, the corresponding mean value for control t_o^{ctrl} and by dividing the result by the reference duration. It read $\overline{\delta t_o} = \left(t_o - t_o^{ctrl}\right)/T$. We repeated the same computation for the positional quantities using control mean embryo length L as reference length for normalizing. For each experiment, we computed the shift of the position of oscillation onset, p_o, or of oscillation die-down, p_d, with respect to the corresponding control mean position p_o^{ctrl} or p_d^{ctrl}, respectively. After normalization, we obtained the normalized shift of the oscillation onset $\overline{\delta p_o} = (p_o - p_o^{ctrl})/L$ and of the die down $\overline{\delta p_d} = (p_d - p_d^{ctrl})/L$. Independently of the quantity used for normalizing, we used a Student t-test to ask whether the linear fit slope was significantly different from 0. Doing so, we ensured distinguishing whether embryo length had an impact on the considered positions or timing, since both means and corresponding standard deviations scaled identically with this normalizing factor.

Bibliography

Jaqaman, K., D. Loerke, M. Mettlen, H. Kuwata, S. Grinstein, S. L. Schmid and G. Danuser (2008). "Robust single-particle tracking in live-cell time-lapse sequences." Nature Methods **5**(8): 695-702.

Kalman, R. E. (1960). "A New Approach to Linear Filtering and Prediction Problems." Journal of Basic Engineering **82**(1): 35-45.

Komarova, Y., C. O. De Groot, I. Grigoriev, S. M. Gouveia, E. L. Munteanu, J. M. Schober, S. Honnappa, R. M. Buey, C. C. Hoogenraad, M. Dogterom, G. G. Borisy, M. O. Steinmetz and A. Akhmanova (2009). "Mammalian end binding proteins control persistent microtubule growth." J Cell Biol **184**(5): 691-706.

Kozlowski, C., M. Srayko and F. Nedelec (2007). "Cortical microtubule contacts position the spindle in C. elegans embryos." Cell **129**(3): 499-510.

Pecreaux, J., S. Redemann, Z. Alayan, B. Mercat, S. Pastezeur, C. Garzon-Coral, A. A. Hyman and J. Howard (2016). "The Mitotic Spindle in the One-Cell C. elegans Embryo Is Positioned with High Precision and Stability." Biophys J **111**(8): 1773-1784.

Pecreaux, J., C. Zimmer and J. C. Olivo-Marin (2006). Biophysical active contours for cell tracking I: Tension and bending. 2006 Ieee International Conference on Image Processing, Icip 2006, Proceedings. October 8-11 2006, Atlanta, GA, USA**:** 1949-1952.

Straube, A. and A. Merdes (2007). "EB3 regulates microtubule dynamics at the cell cortex and is required for myoblast elongation and fusion." Curr Biol **17**(15): 1318-1325.

Supplementary text for the article"Astral microtubule dynamics regulate anaphase oscillation onset and set a robust final position of the *C. elegans* zygote spindle."

Hélène Bouvrais*,[1,2], Laurent Chesneau[1,2], Sylvain Pastezeur[1,2], Marie Delattre[3], and Jacques PECREAUX*,[1,2]

[1]CNRS UMR 6290, 2 avenue du Professeur Léon Bernard, CS 34317, F35043 Rennes cedex France.
[2]University Rennes 1, UEB, SFR Biosit, School of medicine, F-35043 Rennes, France
[3]Laboratory of Molecular Biology of the Cell, Ecole Normale Supérieure de Lyon, CNRS, Lyon, France

February 4, 2017

*To whom correspondence should be addressed: helene.bouvrais@univ-rennes1.fr, jacques.pecreaux@univ-rennes1.fr

Contents

1 Introduction

We aim to complement our previously published "tug–of–war" model (Grill et al., 2005; Pecreaux et al., 2006), mainly focused on the dynamics of cortical force generators, by including the dynamics of astral microtubules (MTs). Indeed, we revealed that the microtubule contacts mostly concentrated in cortical regions close to the centrosomes (Fig. 1). In consequence, the position of the centrosomes, as microtubule organizing centers, regulates through the microtubule dynamics the number of engaged force generators, likely cytoplasmic dynein (Nguyen-Ngoc et al., 2007), pulling on astral microtubules. In turn, it regulates anaphase spindle oscillations and posterior displacement. In a first part, focusing on the oscillation onset, we will neglect the change in force generator processivity along the course of mitosis. We will detail the model and then explore how this novel regulation combines with the one by force generators processivity previously reported (Pecreaux et al., 2006). In a second part, through a stochastic simulation approach, we will look at the feedback loop created between the position of the posterior centrosome and the pulling forces contributing to displacing the spindle, accounting for an evolution of processivity along the course of mitosis.

2 Modelling the positional switch on oscillation onset

2.1 Number of microtubules reaching the posterior crescent of active force generators

Recent work suggested that force generators would be active only on a posterior cap instead of the whole posterior half cortex of the embryo (Krueger et al., 2010). This means that only the microtubules hitting the cortex in this region would contribute to spindle displacement by binding to pulling force generators. We thus aimed to compute the number of microtubules reaching such a so-called *active region/posterior crescent* of the cortex.

2.1.1 Modelling hypotheses and parameter estimates

We reasoned that the number of microtubules reaching the cortex, assumed to be in excess during anaphase (Grill et al., 2005; Pecreaux et al., 2006), could be limiting prior to oscillation onset. Keys to assess this possibility were an estimate of the total number of microtubules and their dynamics. Based on previously published *in vitro* experiments, we assessed microtubule related parameters:

- **Total number of microtubules** To assess the number of nucleation sites at the centrosome, we relied on electron microscopy images of the centrosomes (Redemann et al., 2016), which suggest 3000 or more microtubules. More specifically in the figure 3, authors provide a slice of about 0.85 μm thick (as estimated from video 8) displaying 520 astral microtubules, while centrosome diameter was estimated to 1.5 μm. Only a slice of centrosome was imaged in this assay, so the number of microtubule nucleation sites per centrosome was estimated to a least 1800 by estimating the number for a whole centrosome (a whole sphere). In this work, we set the number of microtubules to $M = 3000$,

as in (O'Toole et al., 2003), although variation of this number within the same order of magnitude does not change our conclusions.

- **The microtubules are distributed around the centrosomes in an isotropic angular fashion** Finally, we hypothesized an isotropic angular distribution of microtubules around the centrosome following (Howard, 2006). This is also suggested though electron microscopy (Redemann et al., 2016).

- **Free-end catastrophes are negligible** With the above estimate of the number of microtubules and with a microtubule growth speed in the cytoplasm $v^+ = 0.67$ μm/s (Srayko et al., 2005) and a shrink one $v^- = 0.84$ μm/s (Kozlowski et al., 2007), we can estimate that about 70 MTs reach the cell periphery (assumed to be at 15 μm from the centrosome) at each second and per centrosome, if the catastrophe rate is negligible. After (Redemann et al., 2016), the vast majority of microtubules emanating of the centrosome are astral: we thus neglected the kinetochore and spindle microtubules in this estimate. Focusing on metaphase and with a residency time of microtubule ends at the cortex of 1.25 s (this work, (Kozlowski et al., 2007)), this leads to about 100 MTs contacting the cortex per centrosome, at any given time. Using our landing assay (Fig. S1C, S2A), we can estimate the number of contacts in the monitored region at any given time to 5 MTs. Extrapolating this to a whole centrosome and assuming the isotropic distribution of astral microtubules (see §2.1.2), we find 26 MTs cortical contacts at any time in metaphase. Although a bit low, likely because of the conservative parameters of the methods (see suppl. exp. proc.) that could lead to missing some microtubules, this estimate is consistent with the one in (Garzon-Coral et al., 2016). A non negligible catastrophe rate would have dramatically reduced that number of contacts at any given time. We concluded that free–end catastrophe rate is negligible.

  Recently, it was proposed that the catastrophe rate could be as high as 0.25 s^{-1} in the mitotic spindle (Redemann et al., 2016). On the one hand, this might be specific to this organelle since the spindle is much more crowded than the cytoplasm. On the other hand, these authors propose a total number of microtubule two to three folds larger. We assert that our conservative estimate of the number of microtubules combined with neglecting free-end catastrophe resulted in similar modeling results, with the advantage of the simplicity over a full astral microtubule model. In other words, we focused on the fraction of astral microtubules not undergoing free–end catastrophe, which is the only fraction mesurable at the cortex.

- **No microtubule nucleation site is left empty at the centrosomes** This is a classic hypothesis (Howard, 2006), recently supported by electron microscopy experiments (Redemann et al., 2016).

2.1.2 Microtubule dynamics "measure" the centrosome–cortex distance.

Probability for a microtubule to reside at the cell cortex Because microtubules spend most of their "lifespan" growing to and shrinking from the cortex, the distance between the centrosomes and the cortex limits the number of microtubules residing at the cortex at any given time. We summarized microtubule dynamics in a single parameter α by writing the fraction of time during which a microtubule resides at the cell cortex:

$$q \;=\; \frac{\tau}{\frac{d}{v^+}+\frac{d}{v^-}+\tau} \;=\; \frac{1}{1+\alpha d} \quad \text{with } \alpha = \frac{1}{v^+\tau}+\frac{1}{v^-\tau}, \tag{1}$$

where d is the distance from the centrosome (microtubule organizing center) to the cortex estimated to $d = 15$ μm (about half of the embryo width). We then estimated $\alpha = 2.15 \times 10^6$ m^{-1} using the above microtubule dynamics parameters. This meant that the microtubule spent $q = 3$ % of its time at the cortex and the remaining time growing and shrinking. This fraction of time spent residing at the cortex is consistent with estimate coming from investigating the spindle centering maintenance during metaphase (Pecreaux et al., 2016).

q can also be seen as the probability for an astral microtubule to reside at the cell cortex. The equation above suggests that it is a measure of the centrosome-cortex distance in "units of microtubule dynamics".

Range of variation of the microtubule contact density at the cortex. The nematode embryo shape is slightly elongated. Therefore, the displacement of the centrosome can vary the centrosome-cortex distance from a factor of 1.5 to 2. We thus wondered whether the dynamics of a microtubule are so that one can observe significant variations of residing probability q. We estimated this sensitivity through the ratio ρ of the probability of reaching the cortex when the centrosome is at its closest position d_1 (set to half of the embryo width, the ellipse short radius) divided by the probability when it is at its furthest position d_2 (chosen as half of the embryo length).

$$\rho = \frac{1+\alpha d_2}{1+\alpha d_1} \tag{2}$$

This curves has a sigmoid–like shape with $\lim_{\alpha\to 0}\rho = 1$ and $\lim_{\alpha\to\infty}\rho = d_2\,/d_1\,$.

Using our measurement of microtubule distribution at the cortex (Fig. S1C, S2A), we sought an experimental estimate of this sensitivity parameter. Because our assay did not enable us to image the very tip of the embryo (Fig S1A), we will have to compare the sensitivity ratio computed from the density map with a theoretical one, not using the half embryo length as maximum distance but the largest distance effectively measurable. When imaging untreated embryo labelled with α-tubulin::YFP, the embryo length in the spindle plane was $2a = 49.2$ μm. In the cortex plane, we measured a length along AP-axis (denoted with bars) $2\bar{a} = 38.0$ μm for the adhering part to the coverslip when imaging at the cortex (Fig. S1A). We can compute the truncation of the ellipse due to the adhesion through the polar angle $\zeta = \arccos(\bar{a}\,/a\,)$ of the boundary of the adhering region. We obtained $\zeta = 39.4°$, which corresponds to a spindle plane to flattened cortex distance of 10 μm, using a parametric representation of the ellipse. During metaphase (the 2 minutes preceding anaphase onset), when the spindle is roughly centered (Pecreaux et al., 2016), the average spindle length is 11.8 μm (N=8 embryos). The furthest visible region is thus at $d_2 = 16.5$ μm while the closest one is at $d_1 = 10$ μm, leading to a sensitivity ratio $\rho = 1.62$ consistent with the microtubule contact density ratio observed on cortex images (Fig. 1, S1C) for *C. elegans*. We concluded that microtubule dynamics in *C. elegans* enable the read-out of the position of the posterior centrosome through the probability of microtubules to reside at the cell cortex.

2.1.3 Number of microtubules reaching the cortex

Since microtubule dynamics were so that it could "measure" the centrosome–cortex distance as a probability of microtubule contacting the cortex, we set to estimate the variation of the total number of contacts for astral microtubules emanating from a single centrosome with the position of this centrosome along the AP-axis. We worked in spherical coordinates (r, θ, ϕ) centered on the posterior centrosome (animated by a slow posterior displacement and assumed as a quasi-static motion), with zenith pointing towards posterior. We denoted θ the zenith angle and ϕ the azimuth (Fig. S3A). We computed the probability of a microtubule to reach the cortex in the active region, represented as $\theta \in [0, \theta_0]$ and $\phi \in [0, 2\pi]$. We integrated over the corresponding solid angle. Then the number of microtubules reaching the cortex $\mathcal{M}(\mathcal{S}, \alpha)$ comes readily (Fig. 2A),

$$p(\mathcal{S}, \alpha, \theta, \phi) = \frac{1}{1 + \alpha\, r_{\mathcal{S}}(\theta, \phi)} \sin(\theta) \tag{3}$$

$$P(\mathcal{S}, \alpha) = \int_{\theta=0}^{\theta_0} \int_{\phi=0}^{2\pi} p(\mathcal{S}, \alpha, \theta, \phi)\, \mathrm{d}\,\phi\, \mathrm{d}\,\theta \tag{4}$$

$$\mathcal{M}(\mathcal{S}, \alpha) = M / 4\pi\, P(\mathcal{S}, \alpha) \tag{5}$$

where $r_{\mathcal{S}}(\theta, \phi)$ is the distance centrosome–cortex in polar coordinates centered on the centrosome, dependent upon the shape of the cortex $\mathcal{S}$ and θ_0 the boundary of the "active force generators region" (Fig. 2C). We observed a switch-like behavior as the posterior centrosome gets out of the cell center and closer to the posterior side of the embryo (Fig. 2A).

2.2 Extended "tug–of–war" model

Because the number of microtubules reaching the cortex could be limiting (Kozlowski et al., 2007), we set to extend the original model of anaphase oscillations. In contrast, in the original "tug–of–war" model (Grill et al., 2005), we had made the assumption that the limiting factor was the number of engaged cortical force generators while, in comparison, the astral microtubules were assumed in excess. It resulted that oscillations were driven by the number and the dynamics of force generators. In the linearized version of the original "tug–of–war" model, the persistence of force generators to pull on microtubules (processivity) mainly governed the timing and frequency of the oscillations, while the number of force generators drove their amplitude (Pecreaux et al., 2006).

2.2.1 The original "tug–of–war" model

We provide here a brief reminder of the "tug–of–war" model (Pecreaux et al., 2006). This model features cortical force generators (stall force $\bar{f}$) exhibiting stochastic binding to and detaching from microtubules at rates k_{on} and $\overline{k_{off}}$ ($\overline{k_{off}}$ the detachment rate at stall force), respectively. The probability for a force generator to be pulling on a microtubule then reads $\bar{p} = k_{on} / \left(k_{on} + \overline{k_{off}}\right)$. The active force generators are distributed symmetrically between

the upper and lower posterior cortices but asymmetrically between anterior and posterior cortices (Grill et al., 2003) (see §2.2.2). We here provide the computation for the symmetric case (along the transverse axis). In the model, we had also included two standard properties of the force generators: firstly, a force-velocity relation $f = \bar{f} - f'\,v$, with f the current force and v the current velocity and f' the slope of the force velocity relation ; secondly, a linearized load dependent detachment rate $k_{off} = \overline{k_{off}}\left(1 - \frac{\bar{f}-f}{f_c}\right)$, with f_c the sensitivity to load/pulling force, assuming that force generator velocity is low, i.e. they act close to the stall force (Pecreaux et al., 2006). We finally denoted Γ the passive viscous drag, related in part to the spindle centering mechanism (Garzon-Coral et al., 2016; Howard, 2006; Pecreaux et al., 2016) and $\bar{N}$ the number of available force generators in the posterior cortex.

A quasi-static linearized model of posterior displacement reads:

$$I(\bar{p})\ddot{y} + (\Gamma - \Xi(\bar{p}))\,\dot{y} + Ky = 0, \tag{6}$$

with

$$\Xi(\bar{p}) = 2\bar{N}\left\{\frac{\bar{f}}{f_c}\bar{p}\left[(1-\bar{p}) - \frac{f_c}{\bar{f}}\right]\right\}\frac{f}{v_0}, \tag{7}$$

and

$$I(\bar{p}) = 2\bar{N}\left\{\frac{\bar{f}}{f_c}\bar{p}\,(1-\bar{p})\right\}\frac{f}{v_0}\frac{\bar{p}}{k_{on}}, \tag{8}$$

Oscillations develop when the system becomes unstable, meaning when so-called *negative damping* $\Xi(\bar{p})$ overcomes the viscous drag.

2.2.2 Evolution of the original "tug–of–war" model to account for polarity encoded through on-rate

When we designed the original model, it was known that the posterior displacement of the spindle was caused by an imbalance in the number of active force generators (Grill et al., 2003), i.e. the number of force generators engaged in pulling on astral microtubules. However, the detailed mechanism building this asymmetry was elusive. We recently investigated the dynamics of dynein at the cell cortex (Rodriguez Garcia et al., 2016) and concluded that an asymmetry in force generator attachment rate (indistinguishably either assembling the trimeric complex (Nguyen-Ngoc et al., 2007) or attaching to microtubule) was the ground of the imbalance, in response to the asymmetric localization of GPR-1/2 (Park and Rose, 2008; Riche et al., 2013). Therefore, to simulate the posterior displacement of the posterior centrosome (see §3), we rather used the equation above with distinct k_{on} on anterior and posterior sides but with equal number of available force generators.

2.2.3 Number of engaged force generators: modelling of microtubule–force-generator binding

To account for the limited cortical anchors (Grill et al., 2005; Pecreaux et al., 2006), we modelled the attachment of a force generator to a microtubule (Nguyen-Ngoc et al., 2007) as a first order process, using the law of mass action on component numbers (Koonce and

Tikhonenko, 2012) and combined it to the number conservation equations for force generators and microtubules.

Force generator–Microtubule attachment modelling

$$K_a = \frac{N_{\text{microtubule–force-generator}}}{N_{\text{free-microtubule-at-cortex}}\, N_{\text{free-force-generator}}} \tag{9a}$$

$$N = N_{\text{Microtubule–force-generator}} + N_{\text{free-force-generator}} \tag{9b}$$

$$M = N_{\text{microtubule–force-generator}} + N_{\text{free-microtubule-at-cortex}} \tag{9c}$$

$$= \mathcal{M}(\mathcal{S}, \alpha) \tag{9d}$$

where N is the total number of force generators present in the posterior crescent (active region).

We could relate the association constant K_a to our previous model (Pecreaux et al., 2006) (see §2.2.1) by writing

$$K_a = \begin{cases} \widehat{k_{on}} \,/\overline{k_{off}} \\ \\ \bar{p}\,/(1-\bar{p})\;/N_{\text{free-microtubule-at-cortex}} \end{cases} \tag{10}$$

with $k_{on} = \widehat{k_{on}} N_{\text{free-microtubule-at-cortex}}$ and $\overline{k_{off}}(t)$ the off-rate thought to depend on mitosis progression. Time dependences were omitted for sake of clarity. It is noteworthy that k_{on} used in the original model as force generator binding rate to microtubules is now variable along the course of mitosis as it depends on the number of free microtubule contacts at the cortex, thus to the position of the centrosome. In contrast, $\widehat{k_{on}}$ is constant representing the real on-rate of the first order reaction.

Related parameter estimate In modelling anaphase oscillation onset, we neglected the variable off-rate along the course of anaphase/mitosis progression (see sections 2.2.6 and 3 for full model without this assumption). The positional switch modelled here limits the number of engaged force generators at oscillation onset. At this time, the number just crosses the threshold to permit oscillations (Pecreaux et al., 2006) and we estimated that 70 % of the force generators are thus engaged, consistent with the quick disappearance of oscillations upon progressively depleting the embryo from GPR-1/2 proteins. We observed that the oscillation starts when the centrosome reaches 71 % of embryo length (Table 1). At that moment, we estimated above the number of microtubules contacting the cortex to 52. We also set the total number of force generators to 50, so that we get a number of engaged ones between 10 and 100 as previously reported (Fig. S6A) (Grill et al., 2003). We thus estimated the association constant $K_a^0 \simeq 0.1$ (denoted with 0 superscript to indicate that we neglected its variation along the mitosis). In turn, we estimated $\widehat{k_{on}} \simeq 0.025\ \text{s}^{-1}$ assuming that the detachment rate at that time was about $4\ \text{s}^{-1}$ (Rodriguez Garcia et al., 2016). If 70 % of the force generators are engaged at oscillation onset, it would correspond to $k_{on} \simeq 0.375\ \text{s}^{-1}$, thus comparable to the estimate used in the original model (Pecreaux et al., 2006).

Modelling the number of engaged force generators in the posterior crescent In the early stages of the mitosis, when the spindle lays in the middle of the embryo (*C. elegans*) or slightly anteriorly (*C. briggsae*), both centrosomes are far from their respective cortex and thus the imbalance in force generator number due to the polarization of the embryo results in a slight posterior pulling force and causes a slow posterior displacement. The closer the posterior centrosome gets to its cortex, the larger the force imbalance (because more microtubules reach the cortex), and the posterior displacement accelerates slightly to (potentially) reach an equilibrium position during metaphase resulting in a plateau in posterior centrosome displacement located around 70 % of the AP-axis. Once anaphase is triggered, the decreased coupling between anterior and posterior centrosomes results into a sudden imbalance in favor of posterior pulling forces and posterior displacement speeds up.

We quantitatively modelled this phenomenon by combining the law of mass action above (eq. 9a) with the number of microtubules reaching the posterior crescent (eq. 5) to obtain the number of engaged force generators in the posterior cortex as following:

$$\begin{aligned} &\mathcal{N}\left(\mathcal{M}\left(\mathcal{S},\alpha\right)\right) = N\frac{\phi-1}{\phi+1} \\ &\quad \text{with} \quad \phi = \zeta^{-} + \sqrt{1+\zeta^{-2}+2\zeta^{+}} \\ &\quad \zeta^{\pm} = K_a\left(\mathcal{M}\left(\mathcal{S},\alpha\right) \pm N\right) \end{aligned} \tag{11}$$

To challenge our model, we tested the switch-like behavior in a broad range of association constants K_a (Fig. S4A). When the posterior centrosome is between 50 % and 70 % of embryo length, we observed that the number of engaged force generators was increased up to a threshold that enables oscillations, consistently with (Pecreaux et al., 2006). When the centrosome is posterior enough, practically above 70 %, the number of engaged force generators saturated, suggesting that their dynamics are now the control parameters (during anaphase then), as proposed in the original "tug–of–war" model. We also observed that a minimal binding constant is required to reach the threshold number of engaged force generators required for oscillations. Interestingly, above this minimal K_a, further increase of the binding constant does not alter significantly the positional switch (Fig. S4A). This suggests that this positional switch operates rather independently of the force generator processivity. This will be further discussed below (§2.2.6).

The positional switch is independent of the total number of force generators, while it is above a threshold As we previously suggested that the total number of force generators should not impact the positional switch (Riche et al., 2013), we computed the corresponding prediction in our model (Fig. S6A) and seek for an experimental confirmation. Up to recently, it was thought that the number of force generators contributing to the posterior displacement was controlled by GPR-1/2 proteins (Colombo et al., 2003; Grill et al., 2003). To keep above the threshold needed for oscillations (Pecreaux et al., 2006), we only decreased partially the number of active force generators in a controlled fashion through a mutation of one of their redundant regulators, GPR-2, using a strain carrying both GFP::α-tubulin transgene and mutation *gpr-2(ok1179)*. Oscillation amplitude was decreased to 7.1 ± 0.9 % of embryo width (N=8, p=1.47×10^{-5}) with respect to control, whose amplitude was 19.2 ± 0.9 %, confirming a reduction of the number of active force generators. In these conditions,

we observed that the oscillations still started when the posterior centrosome reached 70 % of embryo length (Fig. S6C) and slightly later than the control (Fig. S6B). This result supported our model proposing that when the total number of force generators is above the threshold of the original "tug-of-war" model, the position of the centrosome sets the moment of oscillation onset. We recently proposed that the asymmetry in active force generators could be an asymmetry of force generator association rate (called on-rate) to form the trimeric complex that pulls on microtubules (Rodriguez Garcia et al., 2016). GPR-1/2 would increase this on-rate. In our extended model, a decreased on-rate (through *gpr-2* mutant) would result in a decrease association constant K_a. Similarly to the case with an asymmetry in number, above a certain threshold of K_a, the position at which oscillations are set on is not significantly modified (Fig. S4A). In conclusion, independently of the details used to model the polarity (i.e. in number or in on-rate), the mild depletion of GPR-1/2 experiment, causing a reduced number of active force generators, supports our extended model.

To further understand how the various parameters impact this switch-like behavior, we performed a sensitivity analysis using this model (Fig. 2B, S6A, 4A, S4A, S5).

2.2.4 The switch-like behavior of the number of microtubules reaching the cortex *versus* centrosome position is independent of detailed embryo shape

The above results were obtained by assuming an ellipsoidal shape for the embryo (an ellipsoid of revolution around the AP axis, prolate or oblate). We wondered whether a slightly different shape could alter the result. We thus repeated the computation, modelling the embryo shape by a super-ellipsoid of revolution, based on super-ellipses (Lamé curves) (Edwards, 1892) defined as:

$$\left|\frac{X}{a}\right|^n + \left|\frac{Y}{b}\right|^n = 1 \tag{12}$$

with a and b the half length and width, n the exponents and (X, Y, Z) the cartesian axes with X along the AP-axis (long axis), positive values towards the posterior side. We obtained a similar switch-like behavior. (Fig. S3). We concluded the the switch–like behavior observed was robust to changes of the detailed shape and thus performed the remaining investigations with an ellipsoid shape, for sake of simplicity.

2.2.5 Discussion: number– or density–limited force generator – microtubule binding

By writing the law of mass action in protein number (eq. 9a), we have assumed that the force generator–microtubule binding reaction is rate limited but not diffusion limited. We recently investigated the dynamics of cytoplasmic dynein (Rodriguez Garcia et al., 2016), the molecular motor likely pulling on microtubules from the cortex (Nguyen-Ngoc et al., 2007) and observed that dyneins are abundant in cytoplasm, thus 3D diffusion combined to microtubule plus-end accumulation bring enough dynein to the cortex. Therefore, diffusion of dynein to the cortex is not likely to be a limiting factor in binding force generators to the microtubules. However, another member of the trimeric force generating complex, GPR-1/2, essential to generate pulling forces (Grill et al., 2003; Nguyen-Ngoc et al., 2007; Pecreaux et al., 2006), may be limiting. GPR-1/2 is likely localized at the cell cortex prior to assembly

of the trimeric complex (Park and Rose, 2008; Riche et al., 2013), and in low amount leading to a limited number of cortical anchors (Grill et al., 2003, 2005; Pecreaux et al., 2006). We thus asked whether a limiting areal concentration of GPR-1/2 at the cortex could alter our model predictions. We wrote the corresponding law of mass action:

$$\tilde{K}_a = \frac{\text{[Microtubule–force-generator]}}{\text{[Microtubule-at-cortex] [force-generator]}}, \tag{13}$$

with [force-generator] $= \frac{N_{\text{force-generator}}}{S_{activeRegion}}$, $\tilde{K}_a = K_a S_{activeRegion}$ and $S_{activeRegion}$ the surface of posterior crescent, whose border is considered at 70 % of embryo length. Modelling embryo by a prolate ellipsoid of radii 24.6 μm and 15.75 μm, $S_{activeRegion} \simeq 0.147\, S_{embryo} = 610\ \mu\text{m}^{-1}$, with $S_{embryo} \simeq 4100\ \mu\text{m}^2$ the whole embryo surface.

The probability of a microtubule to hit the cortex (see eq. 3 and 5) is modified as follow (modification highlighted in blue):

$$\tilde{\mathcal{M}}\left(\mathcal{S}, \alpha, \theta, \phi\right) = \frac{M}{4\pi} \frac{1}{1 + \alpha\, r_{\mathcal{S}}\left(\theta, \phi\right)} \frac{1}{r_{\mathcal{S}}\left(\theta, \phi\right)^2} \tag{14}$$

We then computed the number of engaged force generators as above and found also a positional switch (Fig. S4B compared to S4A). We concluded that this alternative modelling of force generator–microtubule attachment is compatible with the positional switch that we observed experimentally.

In contrast with the law of mass action in number, when the centrosome is further displaced towards the posterior after passing the posterior switch, there was no saturation in engaged force generators but a decrease. This may suggest that the position of the centrosomes could control the die-down of the oscillations. In such a case, one would expect that die down did not intervene after a fixed delay after anaphase onset, but at a given position. This contrasts with experimental observations upon delaying anaphase onset (Table 1). Therefore, the law of mass action in number appeared to better model our data.

On top of this experimental argument, we estimated the lateral diffusion of the limited cortical anchors, likely GPR-1/2. We estimated the corresponding diffusion limited reaction rate to $k_{on}^D \simeq 1.2 \times 10^5\ \text{s}^{-1}$ after (Freeman and D., 1983; Freeman and Doll, 1983), considering the parameters detailed previously, a diffusion coefficient for GPR-1/2 similar to the one of PAR proteins $D = 0.2\ \mu\text{m}^2/\text{s}$ (Goehring et al., 2011), and a hydrodynamic radius of 5.2 nm (Erickson, 2009). Compared to the on-rate value proposed above (see §2.2.3) $k_{on} \simeq 0.375\ \text{s}^{-1}$, this suggests that lateral diffusion is not limiting. Lateral diffusion may enhance rather than limits the reaction (Adam and Delbruck, 1968). We concluded that the process is limited by reaction, not diffusion, and we considered action mass in number (eq. 9a) in the remaining of this work.

2.2.6 The processivity and microtubule dynamics set two independent switches on force generators: extended "tug–of–war" model

We now implement the effect of microtubule dynamics on the original "tug–of–war". To do so, we let K_a varying with both the processivity $1/\overline{k_{off}}$ and the position of the centrosome.

In the notations of the original model, since we kept $\widehat{k_{on}}$ constant, it meant that k_{on} varied because of changes in the number of microtubule contacts in the posterior crescent, in turn depending on the position of the centrosome. We then sought the pairs $(\overline{k_{off}^c}, x^c)$ so that eq. 6 is critical, i.e. $\Xi^c = \Gamma^t$ (eq. 7), with x^c the critical position of the centrosome along the antero-posterior axis. Because we are on the transverse axis and considered a single centrosome, we used $\Gamma^t = 140$ μN.s/m after (Garzon-Coral et al., 2016) and obtained the diagram reproduced in fig. 2D. It could be seen as a phase diagram. When the embryo trajectory (the orange arrow) crosses the blue line to go into the blue area, the oscillations start. Since this line is diagonal, it suggests that such an event depends upon the position of the posterior centrosome (ordinate axis) and the detachment rate (abscissa), suggesting that two control parameters contribute to make the system unstable and oscillating. Interestingly, when the embryo continues its trajectory in the phase diagram, it crosses the green line, which corresponds to the moment the system becomes stable again, and oscillations are damped out. This critical line is almost vertical indicating that this event depends almost only from the detachment rate, i.e. the inverse of processivity, consistent with the experimental observation. Interestingly, this behavior is maintained despite modest variations in the range of processivity and centrosome position explored during the division (i.e. the precise trajectory of the embryo in this phase diagram). Note that large values of detachment rate are irrelevant as they do not allow posterior displacement of the spindle (Fig. 5). We concluded that two independent switches control the onset of anaphase oscillations and broadly the burst of forces contributing to spindle elongation and posterior displacement.

3 Simulating posterior displacement and final position

Because the cortical pulling forces involved in the anaphase spindle oscillations are also causing the posterior displacement, and because they depend on the position of the posterior centrosome, it creates a feedback loop on the position of the posterior centrosome. Robustness to some parameters revealed by the sensitivity analysis of the oscillation onset may also have a reduced impact on the final position of the centrosome. This final position is essential as it contributes to determine the position of the cytokinesis furrow, a key aspect in an asymmetric division to correctly partition cell fate determinants (Knoblich, 2010; Rappaport, 1971; White and Glotzer, 2012).

3.1 Modeling posterior displacement

To simulate the kinematics of posterior displacement, we considered the "tug–of–war" extended model (§2.2) and a slowly varying binding constant K_a due to the processivity increasing along mitosis progression (§2.2.3). We computed the posterior pulling force, assuming an axi-symmetric distribution of force generators. The projection of the force exerted by the cortical pulling force generators implied a weakening factor because only the component parallel to the AP-axis contributes to displace posteriorly the spindle. To compute it, we assumed that any microtubule contacting the cortex in the active region has an equal probability to attach a force generator. Therefore, we computed the force weakening due to projection by computing the ratio of the force exerted by each microtubule contacting the cortex weighted

by the probability of contact and integrated over the active region. We then divided by the number of contacts computed above. This weakening ratio was then multiplied by the number of bound force generators previously computed (see 11). It reads:

$$\mathcal{F}^{ante|post}\left(x,\overline{k_{off}}\right)=\frac{2\pi\int_{\theta=0}^{\theta_0^{ante|post}}p\left(\mathcal{S},\alpha,x,\theta\right)\cos\theta\,\mathrm{d}\,\theta}{P\left(\mathcal{S},\alpha,x\right)}\times\mathcal{N}\left(\mathcal{S},\alpha,x,K_a^{ante|post}\right)\bar{f}o \quad (15)$$

with θ_0 is the polar angle of the boundary of the active region positioned at x^0_{ante} and x^0_{post}, obtained assuming an ellipsoidal shape for the embryo. $p\left(\mathcal{S},\alpha,x_{ante|post},\theta\right)$ is defined at eq. 3 and $P\left(\mathcal{S},\alpha,x_{ante|post}\right)$ at eq. 4. This equation was used to compute both anterior and posterior forces, with their respective parameters. After Rodriguez Garcia et al. (2016), the force asymmetry is due to an asymmetry of force-generator–microtubule affinity, under the control of GPR-1/2. We accounted for this through an asymmetric attachment constant writing $K_a^{ante|post}=\beta^{ante|post}\widehat{kon}\,/\overline{k_{off}}$.

We then computed the quantities corresponding to the posterior ones based on the original model (see §2.2.1) and put them in the main equation:

$$I^{post}\,\ddot{x}_{post}+\left(\Gamma-\Xi^{post}\right)\dot{x}_{post}+K\,x_{post}-K_{ante}\,x_{ante}=\eta+\mathcal{F}^{post}(x_{post})-F_{ante} \quad (16)$$

with η a white noise modelling the stochastic attachment and detachment of force generators (Nadrowski et al., 2004; Pecreaux et al., 2006). In particular, we used

$$k_{on}=\widehat{k_{on}}\left(\mathcal{M}\left(\mathcal{S},\alpha,x_{post}\right)-\mathcal{N}\left(\mathcal{S},\alpha,x_{post},K_a^{post}\right)\right)$$

and also applied a weakening of anterior force to account for the uncoupling of spindle poles at anaphase onset (Maton et al., 2015; Mercat et al., 2017). We wrote:

$$F_{ante}=\begin{cases}\mathcal{F}_{ante} & \text{if} \quad \overline{k_{off}}>=\overline{k^0_{off}} \quad (17a)\\ \lambda F_{ante} & \text{if} \quad \overline{k_{off}}<\overline{k^0_{off}} \quad (17b)\end{cases}$$

Similarly, centering force (Garzon-Coral et al., 2016; Pecreaux et al., 2016) is weakened

$$K_{ante}=\begin{cases}K & \text{if} \quad \overline{k_{off}}>=\overline{k^0_{off}} \quad (18a)\\ \lambda K & \text{if} \quad \overline{k_{off}}<\overline{k^0_{off}} \quad (18b)\end{cases}$$

We solved this system numerically using trapezoidal rule and backward differentiation formula of order 2 (TR-BDF2 algorithm) (Hosea and Shampine, 1996). Since we linearized the equations and kept the anterior centrosome at a fixed position, we were bound to explore reasonable variation of the parameters when performing the parameter sensitivity analysis (Fig. 5, S7). As a sanity check, we observed that modest variations in the force generator on-rate, thought to translate polarity cues (Rodriguez Garcia et al., 2016), do modulate the final position as expected from experiments (Colombo et al., 2003; Grill et al., 2001). To ensure that our simulation correctly converges to the final position, we varied the spindle initial position and observed no significant change in the final position (Fig. S7E).

3.2 Result and discussion: robustness of the final position to changes in force generator number or dynamics

We previously proposed that the final centrosome position is dictated both by the centering force stiffness and the imbalance in pulling force generation, mainly the number of active force generators on posterior and their processivity (Pecreaux et al., 2006) (Fig. 5, S7CE dashed lines). In contrast, in the extended "tug–of–war" model, when the centrosome enters into the region corresponding to the posterior crescent, more microtubules are close to transverse and less are close to parallel to the AP-axis (Fig. 2C middle and right panel). This is because microtubules are isotropically distributed around the centrosome. Then, it limits the force pulling on the posterior centrosome (Fig. S7A4). As a consequence, the boundary of the active region sets the final position (Fig. S7B) as seen experimentally (Fig. 3A) and (Krueger et al., 2010). In contrast, the force generator number and dynamics become less important and the final position even shows some robustness to the variations in the number and dynamics of the force generators (Fig. 5, S7C).

We noticed that when the posterior crescent boundary is localized at 80 % of embryo length or more posteriorly, the number of microtubules reaching this region when the spindle is close to the cell center is so reduced that it prevents a normal posterior displacement. Together with the observation that when the region extends more anteriorly the final position is anteriorly shifted, it appears that a boundary at 70 % is a value quite optimal to maximize the posterior displacement. Because this posterior displacement is a key to asymmetric division, it would be interesting (but out of the scope of this work) to see whether a maximal posterior displacement is an evolutive advantage, which would then cause a pressure on the active region boundary.

4 Parameters used in modelling and simulations

In this section, we detail the parameters used in the computation of the number of engaged force generators when validating the extended "tug–of–war" model, and also used when simulating the posterior displacement. We based the parameters estimated on the original "tug–of–war" and on experiments performed elsewhere.

parameter	value	Description and estimate
	Original model parameters	
N	50	Number of force generators per half cortex (Grill et al., 2003) (identical on both sides (Rodriguez Garcia et al., 2016)). $N = 38$ when simulating the original "tug–of–war" to ensure a similar posterior displacement as in extended model, all parameters remaining similar.
K	5 μN/m	Centering spring stiffness. Same order of magnitude as (Garzon-Coral et al., 2016; Pecreaux et al., 2006), decreased to account for longer AP- *versus* transverse axis.
k_{on}^{post}	3 s^{-1}	Fixed force generator attachment rate (on-rate) on posterior side, used only in original "tug–of–war" model.
k_{on}^{ante}	2 s^{-1}	Fixed force generator attachment rate (on-rate) on anterior side, used only in original "tug–of–war" model. Value lower than posterior encodes the polarity (Rodriguez Garcia et al., 2016).
x_{ante}	42 %	Fixed anterior centrosome position (in % of embryo length), corresponding to experimental position at anaphase onset.
f_c	1.5 pN	Force generator detachment rate sensitivity to forces (Pecreaux et al., 2006).
f'	3 μN.s/μm	Slope of the force generator force velocity relation (Pecreaux et al., 2006).
$\bar{f}$	6 pN	Force generators stall force (Pecreaux et al., 2006).
η	$\langle \lvert\eta\rvert \rangle = 0$ $\left\langle \lvert\eta\rvert^2 \right\rangle = 0.1\delta(t)$	Stochastic noise modelling the binding and unbinding of force generators.
	Extended tug-of-war model	
a	24.6 μm	Embryo half-length (along AP-axis). Measured in this study.
b	15.75 μm	Embryo half-width (transverse to AP-axis). Measured in this study.
M	3000	Number of microtubules emanating from each centrosome (O'Toole et al., 2003).
α	2.15 μm^{-1}	Microtubule dynamics parameter, corresponding to know growing/shrinking rates (Kozlowski et al., 2007; Srayko et al., 2005) and cortex residency time $\tau = 1.25$ s (this work and (Kozlowski et al., 2007)).
x_{post}^0	70 %	Position of the boundary of active force generator crescent in posterior embryo half (in % of embryo length) (Krueger et al., 2010).

Simulating posterior displacement		
Γ	300 μN.s/m	Damping due to microtubule network (Howard, 2006) and cytoplasm viscosity (Garzon-Coral et al., 2016).
x^0_{ante}	40 %	Position of the boundary of active force generator crescent in anterior embryo half (in % of embryo length). Assumed to correspond to LET-99 domain boundary (Krueger et al., 2010).
λ	0.5	Weakening factor of anterior forces to account for spindle pole uncoupling during elongation (Maton et al., 2015; Mercat et al., 2017).
$\overline{k^0_{off}}$	4 s^{-1}	Force generator off-rate at metaphase to anaphase transition, estimated from (Rodriguez Garcia et al., 2016).
$\overline{k^\infty_{off}}$	2 s^{-1}	Final force generator off-rate (Rodriguez Garcia et al., 2016).
$\overline{k^{init}_{off}}$	10 s^{-1}	Initial force generator off-rate. Detachment rate (off-rate) with time $\overline{k_{off}}(t)$ varies following a sigmoid [2].
β_{post}	15	Affinity factor in posterior half of the cortex, to account for the increased on-rate (Rodriguez Garcia et al., 2016). Set to have a number of active force generators in range 10-100 and twice larger in posterior (Grill et al., 2003).
β_{ante}	7.5	Affinity factor in anterior half of the cortex, to account for the increased on-rate (Rodriguez Garcia et al., 2016).
$\widehat{k_{on}}$	0.025 s^{-1}	Amplitude of the force generators attachment rate to the microtubule in the extended "tug–of–war" model.

References

Adam, G. and Delbruck, M. (1968). Reduction of dimensionality in biological diffusion processes. In Structural Chemistry and Molecular Biology, (Rich, A., Davidson, N. and Pauling, L., eds), pp. 198–215. W. H. Freeman San Francisco.

Colombo, K., Grill, S. W., Kimple, R. J., Willard, F. S., Siderovski, D. P. and Gonczy, P. (2003). Translation of polarity cues into asymmetric spindle positioning in Caenorhabditis elegans embryos. Science *300*, 1957–61.

Edwards, J. (1892). An elementary treatise on the differential calculus, with applications and numerous examples. Macmillan and Co. The Macmillan Company, London, New York,.

Erickson, H. P. (2009). Size and shape of protein molecules at the nanometer level determined by sedimentation, gel filtration, and electron microscopy. Biol Proced Online *11*, 32–51.

Freeman, D. L. and D., D. J. (1983). The influence of diffusion on surface reaction kinetics. The Journal of Chemical Physics *78*, 6002.

[2] Equation reads $\overline{k_{off}}(t) = \overline{k^{init}_{off}} - (1 + \exp(-(t - t_{therm} - t_0)/T)^{-1} \times K_{off}$, with t the time, $t_{therm} = 50$ s the thermatization time, $t_0 = 175$ s the transition time, $T = 70$ s the time width and $K_{off} = \overline{k^{init}_{off}} - \overline{k^\infty_{off}}$ s^{-1} the variation amplitude.

Freeman, D. L. and Doll, J. D. (1983). Langevin analysis of the diffusion model for surface chemical reactions. The Journal of Chemical Physics *79*, 2343.

Garzon-Coral, C., Fantana, H. A. and Howard, J. (2016). A force-generating machinery maintains the spindle at the cell center during mitosis. Science *352*, 1124–7.

Goehring, N. W., Hoege, C., Grill, S. W. and Hyman, A. A. (2011). PAR proteins diffuse freely across the anterior-posterior boundary in polarized C. elegans embryos. J Cell Biol *193*, 583–94.

Grill, S. W., Gonczy, P., Stelzer, E. H. and Hyman, A. A. (2001). Polarity controls forces governing asymmetric spindle positioning in the Caenorhabditis elegans embryo. Nature *409*, 630–3.

Grill, S. W., Howard, J., Schaffer, E., Stelzer, E. H. and Hyman, A. A. (2003). The distribution of active force generators controls mitotic spindle position. Science *301*, 518–21.

Grill, S. W., Kruse, K. and Julicher, F. (2005). Theory of mitotic spindle oscillations. Physical Review Letters *94*, 108104.

Hosea, M. E. and Shampine, L. F. (1996). Analysis and implementation of TR-BDF2. Applied Numerical Mathematics *20*, 21–37.

Howard, J. (2006). Elastic and damping forces generated by confined arrays of dynamic microtubules. Physical biology *3*, 54–66.

Knoblich, J. A. (2010). Asymmetric cell division: recent developments and their implications for tumour biology. Nat Rev Mol Cell Biol *11*, 849–60.

Koonce, M. P. and Tikhonenko, I. (2012). Dynein Motor Mechanisms. In Dyneins : structure, biology and disease, (King, S. M., ed.), pp. xv, 639 p. Academic Press Amsterdam ; Boston 1st edition.

Kozlowski, C., Srayko, M. and Nedelec, F. (2007). Cortical microtubule contacts position the spindle in C. elegans embryos. Cell *129*, 499–510.

Krueger, L. E., Wu, J. C., Tsou, M. F. and Rose, L. S. (2010). LET-99 inhibits lateral posterior pulling forces during asymmetric spindle elongation in C. elegans embryos. J Cell Biol *189*, 481–95.

Maton, G., Edwards, F., Lacroix, B., Stefanutti, M., Laband, K., Lieury, T., Kim, T., Espeut, J., Canman, J. C. and Dumont, J. (2015). Kinetochore components are required for central spindle assembly. Nat Cell Biol *17*, 697–705.

Mercat, B., Pinson, X., Le Cunff, Y., Fouchard, J., Mary, H., Pastezeur, S., Gachet, Y., Tournier, S., Bouvrais, H. and Pecreaux, J. (2017). Micro-fluctuations of spindle length reveal its dynamics over cell division. (in preparation).

Nadrowski, B., Martin, P. and Julicher, F. (2004). Active hair-bundle motility harnesses noise to operate near an optimum of mechanosensitivity. Proc Natl Acad Sci U S A *101*, 12195–200.

Nguyen-Ngoc, T., Afshar, K. and Gonczy, P. (2007). Coupling of cortical dynein and G alpha proteins mediates spindle positioning in Caenorhabditis elegans. Nature Cell Biology *9*, 1294–1302.

O'Toole, E. T., McDonald, K. L., Mantler, J., McIntosh, J. R., Hyman, A. A. and Muller-Reichert, T. (2003). Morphologically distinct microtubule ends in the mitotic centrosome of Caenorhabditis elegans. J Cell Biol *163*, 451–6.

Park, D. H. and Rose, L. S. (2008). Dynamic localization of LIN-5 and GPR-1/2 to cortical force generation domains during spindle positioning. Developmental Biology *315*, 42–54.

Pecreaux, J., Redemann, S., Alayan, Z., Mercat, B., Pastezeur, S., Garzon-Coral, C., Hyman, A. A. and Howard, J. (2016). The Mitotic Spindle in the One-Cell C. elegans Embryo Is Positioned with High Precision and Stability. Biophys J *111*, 1773–1784.

Pecreaux, J., Roper, J. C., Kruse, K., Julicher, F., Hyman, A. A., Grill, S. W. and Howard, J. (2006). Spindle oscillations during asymmetric cell division require a threshold number of active cortical force generators. Current Biology *16*, 2111–22.

Rappaport, R. (1971). Cytokinesis in animal cells. Int Rev Cytol *31*, 169–213.

Redemann, S., Baumgart, J., Lindow, N., Fuerthauer, S., Nazockdast, E., Kratz, A., Prohaska, S., Brugues, J., Shelley, M. and Mueller-Reichert, T. (2016). Kinetochore Microtubules indirectly link Chromosomes and Centrosomes in C. elegans Mitosis. BioRxiv *060855*.

Riche, S., Zouak, M., Argoul, F., Arneodo, A., Pecreaux, J. and Delattre, M. (2013). Evolutionary comparisons reveal a positional switch for spindle pole oscillations in Caenorhabditis embryos. Journal of Cell Biology *201*, 653–62.

Rodriguez Garcia, R., Chesneau, L., Pastezeur, S., Roul, J., Tramier, M. and Pecreaux, J. (2016). Dynamics of dynein at microtubule plus-ends and the cortex during the division of the c. elegans zygote. (submitted).

Srayko, M., Kaya, A., Stamford, J. and Hyman, A. A. (2005). Identification and characterization of factors required for microtubule growth and nucleation in the early C. elegans embryo. Dev Cell *9*, 223–36.

White, E. A. and Glotzer, M. (2012). Centralspindlin: At the heart of cytokinesis. Cytoskeleton (Hoboken) *69*, 882–92.